ANALYSIS OF THE TECHNIQUES FOR MEASURING PARTICLE SIZE AND DISTRIBUTION FROM FRAUNHOFER DIFFRACTION PATTERNS

Ronald A. Belz

ARO, Inc.

September 1968

ARNOLD ENGINEERING DEVELOPMENT CENTER
AIR FORCE SYSTEMS COMMAND
ARNOLD AIR FORCE STATION, TENNESSEE

NOTICES

When U. S. Government drawings specifications, or other data are used for any purpose other than a definitely related Government procurement operation, the Government thereby incurs no responsibility nor any obligation whatsoever, and the fact that the Government may have formulated, furnished, or in any way supplied the said drawings, specifications, or other data, is not to be regarded by implication or otherwise, or in any manner licensing the holder or any other person or corporation, or conveying any rights or permission to manufacture, use, or sell any patented invention that may in any way be related thereto.

Qualified users may obtain copies of this report from the Defense Documentation Center.

References to named commercial products in this report are not to be considered in any sense as an endorsement of the product by the United States Air Force or the Government.

ANALYSIS OF THE TECHNIQUES FOR MEASURING PARTICLE SIZE AND DISTRIBUTION FROM FRAUNHOFER DIFFRACTION PATTERNS

Ronald A. Belz
ARO, Inc.

AF—AEDC
Arnold AFS Tenn

FOREWORD

This report was originally prepared as a thesis for partial fulfillment of the requirements for a Master of Science degree at the University of Tennessee Space Institute (UTSI), Tullahoma, Tennessee in May 1968.

The research reported herein was sponsored by Headquarters, Arnold Engineering Development Center (AEDC), Air Force Systems Command (AFSC), under Contract F40600-69-C-0001 with ARO, Inc. (a subsidiary of Sverdrup & Parcel and Associates, Inc.), contract operator of AEDC, AFSC, Arnold Air Force Station, Tennessee, under ARO Project No. BC5919.

The work was performed under Program Element 6240533F, Project 8219, Task 821907. The manuscript was submitted for publication on May 20, 1968.

The author wishes to express appreciation to Dr. J. D. Trolinger and P. R. Gault of ARO, Inc., and Dr. F. M. Shofner (committee chairman) and S. Brahmavar of UTSI for their advice and assistance.

This technical report has been reviewed and is approved.

Marshall K. Kingery
Research Division
Directorate of Plans
and Technology

Edward R. Feicht
Colonel, USAF
Director of Plans
and Technology

ABSTRACT

The location and size of particles within a volume which is stationary or dynamic can be found by two techniques of coherent optics. In the first technique the volume is illuminated with coherent light and the resulting diffraction patterns are recorded in the far-field (Fraunhofer region) of the particles. The particle information is found from the resultant density variations on the film. In the second technique the developed negative (a Fraunhofer hologram) is illuminated with coherent light and the particle field is reconstructed in three dimensions. This investigation is an analysis of these two techniques and their relative merits. Because magnification is important in the second technique the methods of magnifying the volume are discussed. It is found that reconstructing the volume from the hologram yields particle information which is easier to obtain than the information resulting from the diffraction patterns. The volume is also found to be easily and uniformly magnified by an imaging lens in the reconstruction process.

CONTENTS

PAGE

I. INTRODUCTION 1

II. FRAUNHOFER DIFFRACTION PATTERNS 5

Introduction 5

Derivation of the Fraunhofer Diffraction Pattern for an Opaque Circular Particle 6

Analysis of the Theoretical Data 11

Calculating the recording distance 18

Calculating particle diameter 19

Experimental Results 21

General experimental considerations 21

Experimental recording distance and particle size calculations 29

Concluding Remarks 33

III. FRAUNHOFER HOLOGRAMS 35

Theoretical Analysis 37

Experimental Data 42

Fraunhofer Hologram Limitations 46

Particle size limits 46

Recording distance 49

Depth of field 52

Out-of-focus images 54

PAGE

IV. MAGNIFICATION OF THE PARTICLE FIELD. 56

Introduction 56

Magnification in the Recording Process 59

Spherical waves. 59

Thin lenses. 61

Magnification in the Reconstruction Process. . . . 65

Spherical waves. 65

Thin lenses. 68

V. SUMMARY AND CONCLUSIONS. 71

BIBLIOGRAPHY 79

ILLUSTRATIONS

FIGURE PAGE

1. Diffraction and Observation Planes for Fraunhofer Diffraction About an Opaque Particle. . 8
2. Theoretical Fraunhofer Diffraction Patterns of the Intensity, I, versus the Position Vector, ρ, for a Fixed Particle Diameter of 160 μm and Z = 4.1, 12.1 and 20.2 cm with λ = 6328 Å. . . 13
3. Theoretical Fraunhofer Diffraction Patterns for a Constant Far-Field Number, N = 3, with a = 40, 80, and 160 μm, Z = 3.0, 12.1, and 48.5 cm, Respectively, and λ = 6328 Å 16
4. Theoretical Fraunhofer Diffraction Patterns for Z = 20 cm, λ = 6328 Å, and Particle Radii of 160, 80, and 40 μm, Respectively 17
5. Approximation Error in the Recording Distance Calculation. 20
6. Schematic Arrangement for Recording Fraunhofer Diffraction Patterns 22
7. Fraunhofer Diffraction Patterns of Black Paint Particles Recorded at Z = 15 cm on SO-243 Film, λ = 6328 Å 24
8. Fraunhofer Diffraction Patterns of a Two-Dimensional Particle Field 25

FIGURE PAGE

9. Theoretical and Experimental Intensity Curves of a 280 μm Diameter Particle Recorded at Z = 15 cm with λ = 6328 Å. 26
10. Theoretical and Experimental Intensity Curves of a 130 x 150 μm Particle Recorded at Z = 15 cm with λ = 6328 Å. 27
11. Theoretical and Experimental Intensity Curves of a 210 μm Diameter Particle Recorded at Z = 10 cm with λ = 6328 Å. 28
12. Theoretical and Experimental Intensity Curves of a 230 μm Diameter Particle Recorded at Z = 40 cm with λ = 6328 Å. 30
13. Reconstructed Image Fields From a Fraunhofer Hologram 36
14. Effects of a Positive Thin Lens on a Plane Wave . . 40
15. Opaque Two-Dimensional Particle Field and the Reconstructed Real Image From a Fraunhofer Hologram 43
16. Reconstructed Real Images From a Fraunhofer Hologram of Two Planes Separated by 5 cm 45
17. Schematic Arrangement for Recording an In-Line Fraunhofer Hologram of Opaque Paint Particles. . . 47
18. Reconstructed Image Planes From a Fraunhofer Hologram of a Spray Paint Volume 48

FIGURE PAGE

19. Dependence of Recording Distance and Volume Depth on Particle Size and Density for Clean Reconstructions from Fraunhofer Holograms. 51

20. Magnification of the Particle Field Using Spherical Waves in Recording and Reconstruction. 57

21. Magnification of a Planar Particle Field by Spherical Wave Recording of a Fraunhofer Hologram where m = 3x. 60

22. Fraunhofer Hologram Construction Using a Lens to Premagnify the Particle Field 63

23. Magnification of a Planar Particle Field in the Recording Process with a Lens where m = 6.4x . 64

24. Real Image of a Planar Particle Field Reconstructed and Magnified 13.5 times with Spherical Waves. . . 67

25. Graphite Particle Field Recorded and Reconstructed with Plane Waves and Magnified During Reconstruction with a Lens System. 69

NOMENCLATURE

a	Particle radius
A	Particle scattering cross-section
A_1	Magnitude of the reference wavefront
A_2	Magnitude of the object wavefront
Å	Angstrom (10^{-10} meters)
b	Film fog level constant
c	Radius of the illuminating plane wave
$D(\bar{\xi})$	Particle geometry
$D(\bar{\alpha})$	Reconstructed particle geometry
$\mathfrak{D}(\bar{\xi})$	Fourier transform of $D(\bar{\xi})$
e	Base of the natural logarithm
f	Focal length
i	$\sqrt{-1}$
I	Intensity at the recording plane
$I(\bar{\alpha})$	Intensity in the image plane
I_o	Incident light intensity
J_1	First order Bessel function
k_1	Wave number of the recording wavefront
k_2	Wave number of the reconstructing wavefront
K	Plane wave amplitude
ℓ	Object distance from a lens
ℓ'	Image distance from a lens
L	Mean free path

L	Lens distance from the recording plane
m	Magnification
m_ℓ	Lens magnification
m_s	Spherical wave magnification
n	Particle density
N	Far-field number
R_1	Distance from the lens focal point to the object field
R_2	Distance from the lens focal point to the hologram
$T(\rho)$	Film amplitude transmittance
$U(\bar{\rho})$	Light distribution in the recording plane
$U(\bar{\xi})$	Light distribution in the object plane
z	Volume depth
Z	Recording distance
Z_2	Reconstruction distance
Z'	Distance from the point source to the object plane
$\bar{\alpha}$	Image plane position vector
γ	Linear portion of the film characteristic curve
λ	Wavelength
μm	Micron (10^{-6} meters)
$\bar{\xi}$	Position vector in the object plane
$\bar{\rho}$	Position vector in the observation, or recording plane
φ	Phase introduced by a lens
φ_1	Phase of the reference wavefront
φ_2	Phase of the object wavefront
∂	Partial derivative

SECTION I
INTRODUCTION

Within the past few years, two techniques of coherent optics have been developed whereby the sizes and spatial distribution of a volume of particles may be recorded on film in the form of diffraction patterns. These techniques have the advantages that the particle field information can be recorded without disturbing the ensemble and that the information may be analyzed at a more convenient time. Unlike conventional methods, which, moreover, are too slow for satisfactorily sampling a dynamic particle field, these techniques are capable of recording the position and size of each particle in the field without having the depth of field problem associated with high resolution photography or microscopy (1).[1]

In the first technique, the Fraunhofer diffraction patterns of the individual particles are recorded on film. These patterns are formed when the particle field is illuminated with coherent, quasi-monochromatic light and the recording plane is in the far-field of the individual

[1]Numbers in parentheses correspond to similarly numbered references listed in the bibliography.

particles. The light diffracted by each particle interferes with the undiffracted beam to produce a fringe pattern characteristic of the particle size and distance from the recording plane. The relation of these particle parameters to the recorded intensity distribution has been derived theoretically for opaque and transparent, circular particles using the far-field assumptions (2,3). From this it has been suggested that "an accurate value of Z and . . . a precise determination of the particle size" (3) may be calculated from microdensitometer traces of the photographically recorded patterns. Section II of this investigation will critically cover the accuracy of this statement.

The diffraction pattern technique was used by Ward (4) to measure the size and distribution of particles in a fog with a Laser Fog Disdrometer. A Q-spoiled ruby laser was the illuminating source. Particles were sized by analyzing the microdensitometer traces of the recorded fringe patterns.

The second technique for measuring the size and location of particles within a volume follows directly from the first. The diffraction patterns recorded on the film comprise an in-line Fraunhofer hologram of the volume (5). Illuminating the hologram with a beam of coherent light will reconstruct the particle field as it was recorded and measurements may be taken from the reconstruction (6,7).

This was the first successful and useful holographic

technique for solving a technological problem (8). It was incorporated into the Laser Fog Disdrometer for reading out the particle information (9). The new readout system used a television camera to image and magnify the particle reconstructions to a measurable size.

When a particle field is to be studied, the relative merits of each technique are important. Errors and approximations in calculating and measuring the particle size and location must be known. These two techniques will be described and discussed in this investigation. This has not been done explicitly in the open literature.

The discussion in Section II will cover the Fraunhofer diffraction pattern technique. After a derivation for the intensity in the far-field, the effects of particle size and recording distance on the intensity patterns will be discussed. From this, expressions for the particle radius and distance from the recording plane will be derived. The diffraction patterns and calculations will be experimentally verified.

The reconstruction of the particle field from the Fraunhofer diffraction patterns will be covered in Section III. A general, but fundamental, description of the reconstruction process will be given and related to the Fraunhofer patterns. Reconstructions from holograms of stationary and dynamic particle fields illuminated by a cw He-Ne laser will be analyzed.

A necessary part of any small particle reconstruction scheme is magnification. Besides electronic magnification with a television camera, as was used on the Laser Fog Disdrometer, the images can also be magnified optically with lenses and with spherical waves (10). Conditions under which each of these would be preferable are important. Because spherical waves and lenses are basic magnification tools, Section IV will explain how each is utilized in recording and reconstructing the hologram and where each would be most suitable. Comparative conclusions relevant to measuring small particle positions and sizes will be made in Section V.

SECTION II
FRAUNHOFER DIFFRACTION PATTERNS

2.1 INTRODUCTION

When a volume of particles is illuminated by coherent light, a portion of the light is diffracted by each particle and interferes with the undiffracted light. By applying the proper boundary conditions of the particle to the Helmholtz-Kirchhoff diffraction integral, the intensity distribution (interference pattern) in a plane a distance Z from the particle can be found. This integral is evaluated under the conditions that the recording plane is in the far field of the particle (the Fraunhofer region) and the near field of the volume. From the resulting intensity distribution, the size of the particles and their respective distances from the recording plane can be calculated.

This Section presents the theoretical derivation of the Fraunhofer diffraction patterns of circular opaque particles. Following an analysis of the derived intensity pattern, the experimentally recorded data will be correlated with the theory. Conclusions drawn from the theory and experimental data will be given.

2.2 DERIVATION OF THE FRAUNHOFER DIFFRACTION PATTERN FOR AN OPAQUE CIRCULAR PARTICLE

Fraunhofer diffraction patterns are formed when the distance from the point source to the object plane, Z', and the distance from the object plane to the recording plane, Z, are such that

$$Z' >> \frac{(\xi^2 + \eta^2)_{max}}{\lambda} \tag{1A}$$

$$Z >> \frac{(\xi^2 + \eta^2)_{max}}{\lambda} \tag{1B}$$

where $(\xi^2 + \eta^2)_{max}$ is the maximum dimension of the diffracting object and λ is the wavelength of the point source (11). By using a collimated light beam the first restriction can be neglected. The second restriction has been shown to be relaxed for circular apertures of diameter 2a when (12)

$$Z \geq \frac{(2a)^2}{\lambda} \tag{2}$$

For other geometries, 2a represents the maximum dimensions of the object. The equality in Equation 2 will be defined as one far-field distance, N, from the particle. Therefore, the recording distance, Z, defined in terms of far-field distances, is

$$Z = N\frac{(2a)^2}{\lambda} \tag{3}$$

The distribution of the light in the recording plane is given by the scalar Helmholtz-Kirchhoff formula as (11)

$$U(\bar{\rho}) =$$

$$\frac{1}{4\pi}\int_S \left\{U(\bar{\xi})\,\frac{\partial}{\partial n}\left(\frac{e^{ikr}}{r}\right) - \frac{e^{ikr}}{r}\,\frac{\partial}{\partial n}\left(U(\bar{\xi})\right)\right\} dS \tag{4}$$

where $U(\bar{\xi})$ is the light distribution in the object plane, r is the magnitude of the vector from the object plane to the observation plane, and $\frac{\partial}{\partial n}$ is the normal derivative to the object plane. The integral is taken over the surface of the object plane.

For the analysis it is assumed that there is an opaque particle in the $\bar{\xi}$-plane as shown in Figure 1 where the geometry of the particle is described by

$$D(\bar{\xi}) = \begin{cases} 1 & |\bar{\xi}| \leq a \\ 0 & |\bar{\xi}| > a \end{cases} \tag{5}$$

where a is the radial dimension of the object and is much larger than λ. For a particle illuminated with a plane wave of amplitude K, the light distribution $U(\bar{\xi})$, in the object plane is given by the boundary condition

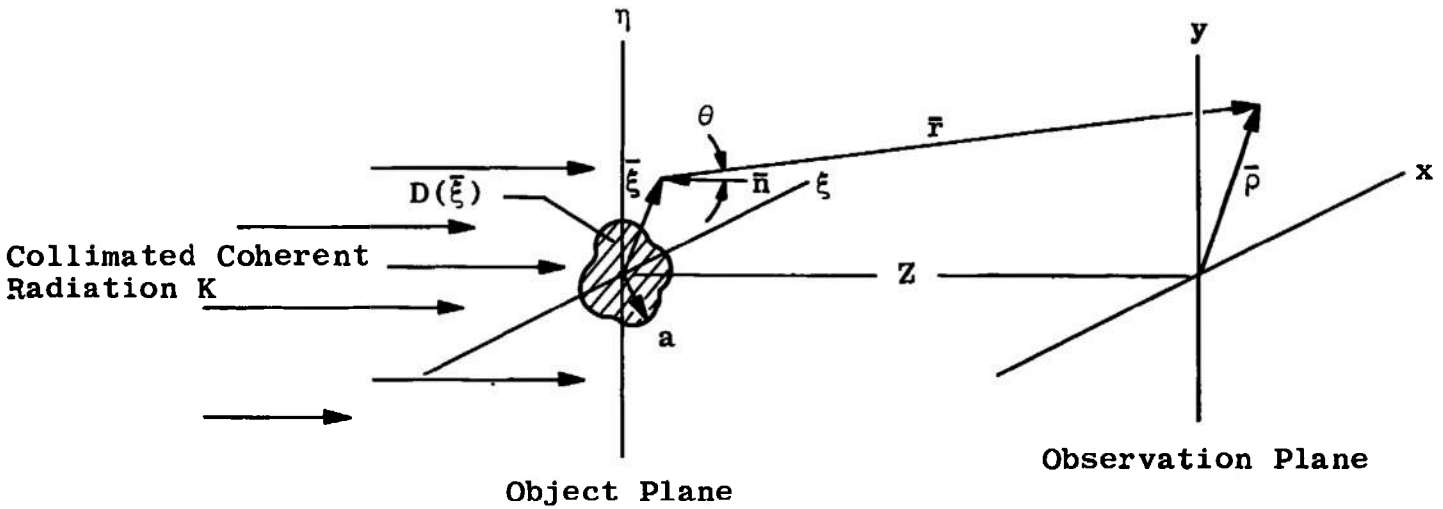

Fig. 1 Diffraction and observation planes for Fraunhofer diffraction about an opaque particle

$$U(\bar{\xi}) = K\left(1 - D(\bar{\xi})\right) \tag{6}$$

Substituting this Equation and its normal derivative into Equation 4 and carrying out the normal derivative within the integral along r gives

$$U(\bar{\rho}) = \frac{K}{4\pi}\left[\int (1)\,\frac{e^{ikr}}{r^2}\,(1 - ikr)\cos\theta\; d\bar{\xi} - D(\bar{\xi})\,\frac{e^{ikr}}{r^2}\,(1 - ikr)\,\cos\theta\; d\bar{\xi}\right] \tag{7}$$

where $\frac{\partial}{\partial n} = \frac{-\partial}{\partial r}\cos\theta$, θ is the angle between the normal to the $\bar{\xi}$-plane and $\bar{r}$ as shown in Figure 1 and the surface integral is taken over the $\bar{\xi}$-plane.

The first integral is evaluated under the near field condition

$$Z \ll kc^2 \tag{8}$$

where c is the radius of the illuminating beam which is also the limiting aperture of the system. This integral then becomes e^{ikZ} which is the undiffracted portion of the plane wave along the Z axis (3).

The second integral can be simplified by assuming that $kr \gg 1$, and imposing the customary paraxial approximations, that is, the diffracted rays are approximately parallel to the Z axis, so that $\cos\theta = \frac{Z}{r} \approx 1$. Under this simplification, Equation 7 becomes (after normalizing the constants in

front of the equation)

$$U(\bar{\rho}) = e^{ikZ}\left[1 + \frac{ik}{Z}\int D(\bar{\xi})e^{ikr}d\bar{\xi}\right] \tag{9}$$

Expanding r inside the integral in a binomial series where

$$r^2 = Z^2 + |\bar{\rho} - \bar{\xi}|^2 \tag{10}$$

dropping the higher order terms of Z^{-2}, and recognizing that in the far-field,

$$k|\bar{\xi}|^2 << Z \tag{11}$$

Equation 9 reduces to

$$U(\bar{\rho}) = e^{ikZ}\left[1 + \frac{ik}{Z}\exp\left[\frac{ik|\bar{\rho}|^2}{2Z}\right]\int D(\bar{\xi})e^{-ik(\bar{\xi}\cdot\bar{\rho})/Z}d\bar{\xi}\right] \tag{12}$$

The intensity in the observation plane is

$$I(\bar{\rho}) = |U(\bar{\rho})|^2 =$$

$$1 - \frac{2k}{Z}\sin\left(\frac{k|\bar{\rho}|^2}{2Z}\right)\left[\tilde{D}(\bar{\rho})\right] + \frac{k^2}{Z^2}\left[\tilde{D}(\bar{\rho})\right]^2 \tag{13}$$

where the background has been normalized and

$$\tilde{D}(\bar{\rho}) = \int D(\bar{\xi})\exp\left[\frac{-ik(\bar{\xi}\cdot\bar{\rho})}{Z}\right]d\bar{\xi} \tag{14}$$

This is the Fourier transform of the particle in the object plane. For a circular particle of radius a,

$$\tilde{D}(\bar{\rho}) = \frac{a^2 J_1\left(\frac{ka\bar{\rho}}{Z}\right)}{\left(\frac{ka\bar{\rho}}{Z}\right)} \tag{15}$$

which is a Bessel function of the first kind divided by its argument and is characteristic of circular particles. The intensity in the recording plane is therefore

$$I(\rho) = 1 - \frac{2ka^2}{Z}\sin\left(\frac{k\rho^2}{2Z}\right)\left[\frac{J_1\left(\frac{ka\rho}{Z}\right)}{\left(\frac{ka\rho}{Z}\right)}\right] + \frac{k^2a^4}{Z^2}\left[\frac{J_1\left(\frac{ka\rho}{Z}\right)}{\left(\frac{ka\rho}{Z}\right)}\right]^2 \tag{16}$$

Because of the circular particle, symmetry has been assumed in the observation plane allowing the vector notation to be dropped.

2.3 ANALYSIS OF THE THEORETICAL DATA

Equation 16 illustrates the effects of the particle size and distance from the film plane on the intensity distribution in the observation plane. The first term, a normalized constant, is due to the background light and sets the average value of the recorded light intensity. The third term is recognized as the Airy diffraction pattern associated

with a circular aperture of radius a (11). It is considered to be an error term in the intensity pattern. The middle term contains the information necessary to obtain the particle size and recording distance from the diffraction pattern. It represents the interference between the coherent background and the light diffracted by the particle. It consists of a sine function dependent only upon the recording distance and a diffraction term characteristic of the particle. The sine function is the dominant term and produces diffraction rings analagous to a Fresnel zone plate. In holographic terminology it is known as the focusing term (13) since the diffraction rings have approximately the same imaging properties as a lens of focal length Z. The sine varies more rapidly than the Bessel function and is, therefore, modulated by it.

This modulation is illustrated by the theoretical diffraction patterns in Figure 2. The vertical dashed lines indicate the points where the Bessel function goes to zero. These points are related to the Airy minima and produce a phase reversal in the intensity pattern. The data in Figure 2 were obtained from a computer program of Equation 16, where a = 80 μm, λ = 6328 Å and Z = 4.1, 12.1, and 20.2 cm respectively. These Fraunhofer patterns illustrate the effects of the sine and Bessel functions on the intensity in the recording plane at one, three and five far-fields from

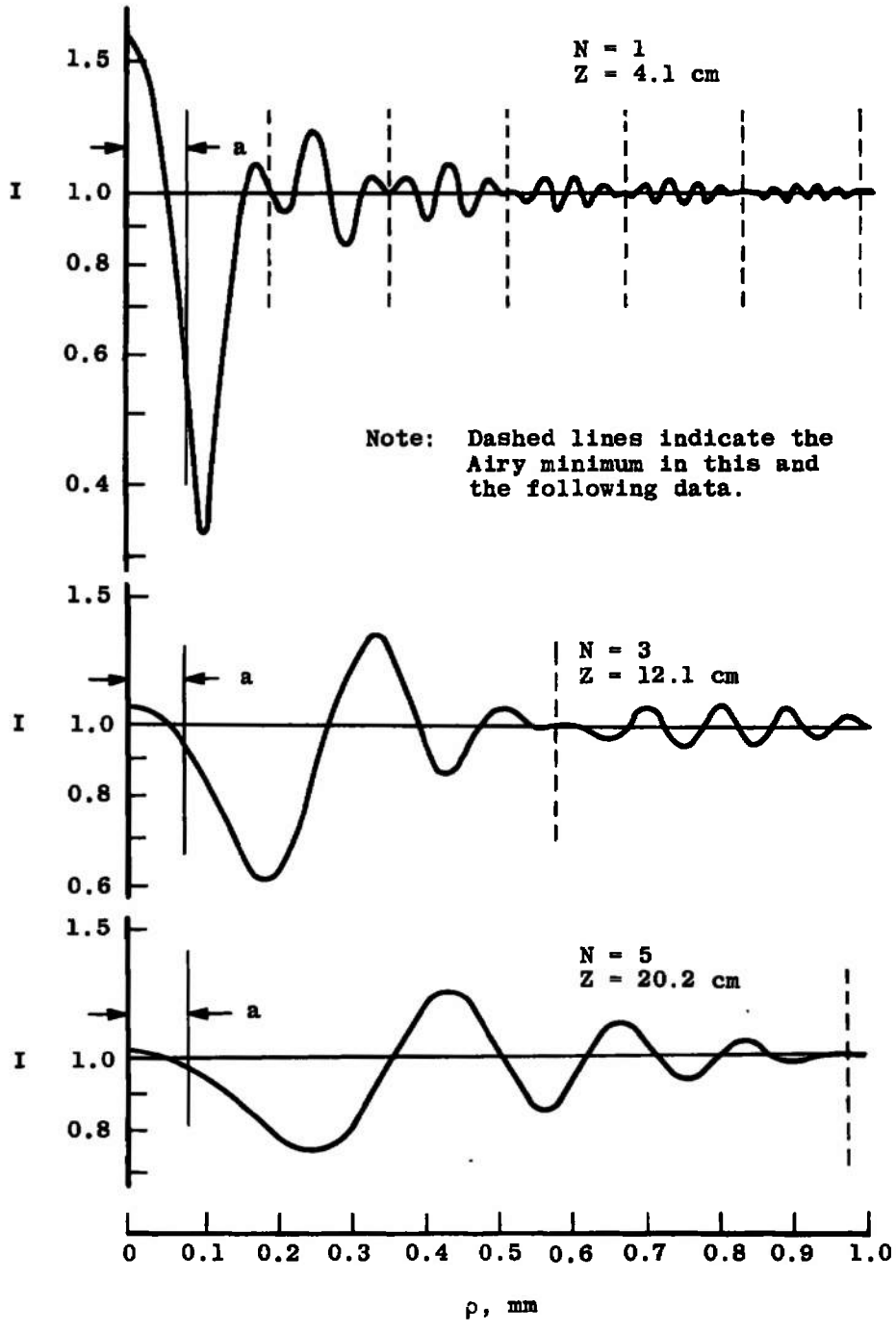

Fig. 2 Theoretical Fraunhofer diffraction patterns of the intensity, I, versus the position vector, ρ, for a fixed particle diameter of 160 μm and Z = 4.1, 12.1, and 20.2 cm with λ = 6328 Å

the particle. More sine peaks are seen to be present within the first Airy minimum as N increases. Likewise, the spatial frequency of the sine term decreases for large far-field distances.

The number of sine peaks within the Airy minimum is a function of the far-field number. Setting the argument of the Bessel function in Equation 15 equal to its value at the first zero and solving for the magnitude of the position vector in the recording plane yields

$$\rho = 0.61\lambda \frac{Z}{a} \tag{17}$$

For $\lambda = 6328$ Å,

$$\rho = 3.86 \frac{Z}{a} \times 10^{-7} \text{ meters} \tag{18}$$

At this value of ρ, the argument of the sine function has a value $\frac{n\pi}{2}$ where n, by definition, is a positive number that describes the number of quadrants or fraction thereof through which the sine has passed. Setting the sine function equal to this value and solving for n yields

$$n = \frac{2\rho^2}{\lambda Z} \tag{19}$$

Substituting Equation 18 into this Equation and using the

far-field relation given by Equation 3, gives

$$n = 2.98N \tag{20}$$

The peaks of the intensity function occur approximately when the sine is maximum; that is, when n is an odd integer. Therefore, the number of sine peaks within the Airy minimum is directly proportional to the number of far-fields at which the diffraction pattern is recorded. For a constant far-field number, the diffraction patterns will look the same with the exception that the frequency increases for small a. This is illustrated in Figure 3. This figure shows the effects of constant N on the intensity distribution for three different particle sizes. As the particle radius increases, Z must also increase in the same proportion. It can be seen that the Airy minimum occurs at the same point on the sine pattern. It should be noticed that the intensity of the peaks of the three patterns are the same since the parameters preceding the second and last terms of the intensity distribution in Equation 16 can be expressed in terms of N^{-1} (6).

When various size particles are recorded in the same plane, the larger particles have more pronounced intensity variations than the smaller ones, with the Airy minimum occurring closer to the center of the pattern, as shown in Figure 4. The spatial frequency for each particle is seen to be approximately the same. Particle radii of 40, 80 and 160 μm, 20 cm from the recording plane, with λ = 6328Å are shown.

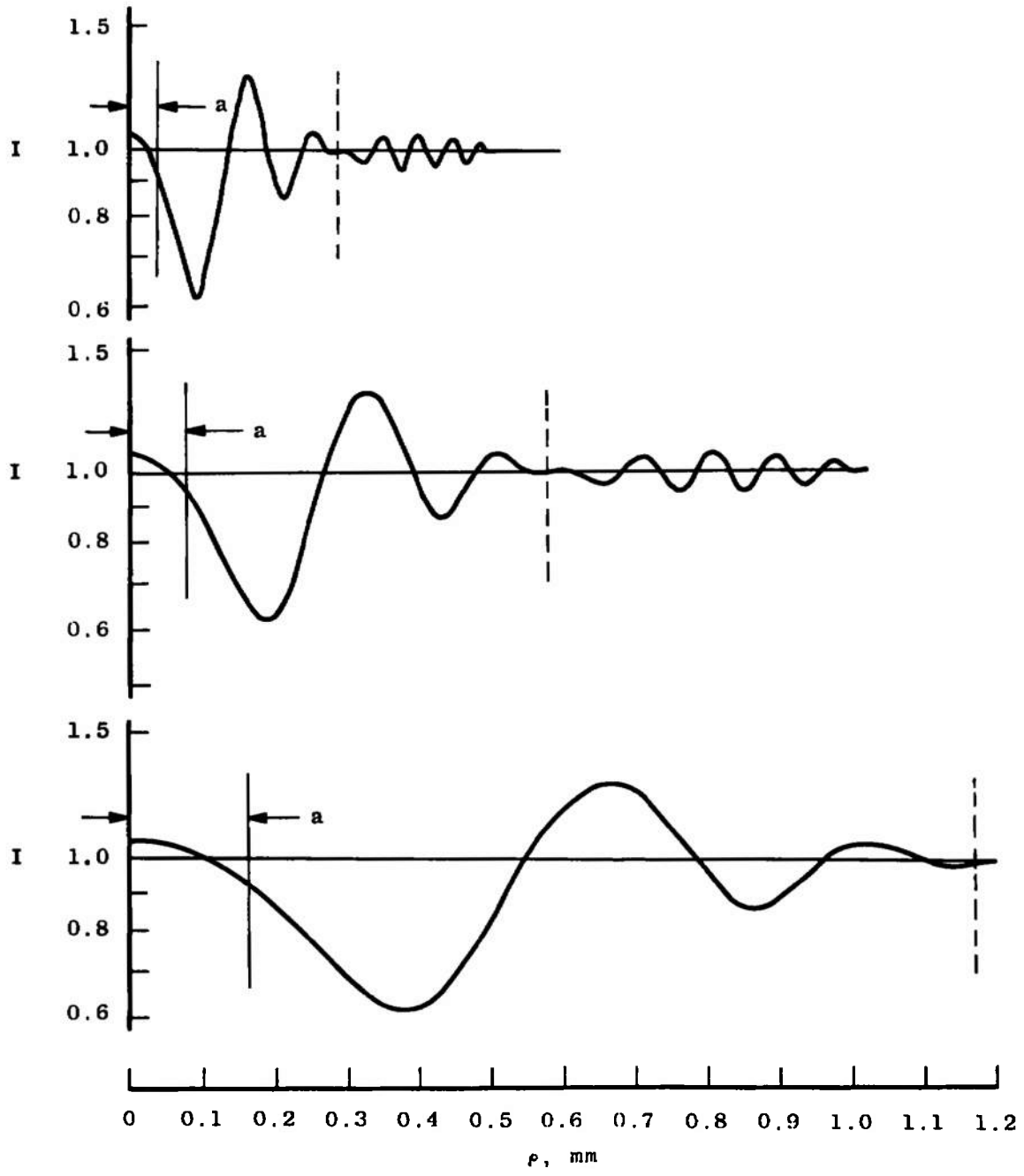

Fig. 3 Theoretical Fraunhofer diffraction patterns for a constant far-field number, N = 3, with a = 40, 80, and 160 μm, Z = 3.0, 12.1, and 48.5 cm, respectively, and λ = 6328 Å

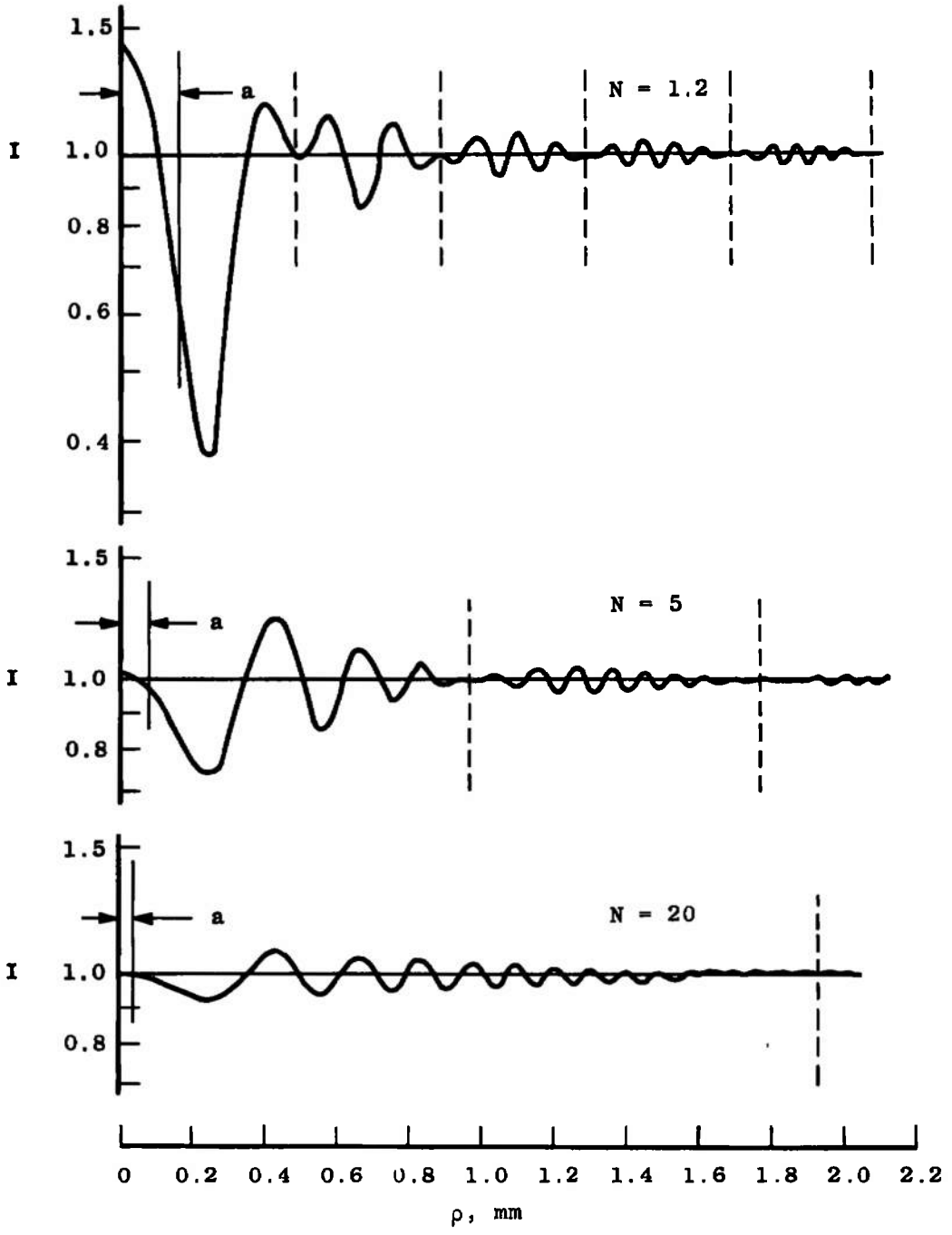

Fig. 4 Theoretical Fraunhofer diffraction patterns for Z = 20 cm, λ = 6328 Å, and particle radii of 160, 80, and 40 μm, respectively

Calculating the Recording Distance

The sine function in Equation 16 was found to be a function of the recording distance Z and independent of the particle size. Therefore, the approximate position of the particle can be found from the sinusoidal variations of the recorded intensity patterns by measuring the distance, ρ, from the center of the diffraction pattern to one of the sine extrema. These extrema occur when the sine function is approximately ± 1. Letting n in Equation 19 be an odd integer specifying the maxima or minima of the sine function and solving for Z yields

$$Z = \frac{2\rho^2}{n\lambda} \quad , \quad n = 1,3,5,\cdots \tag{21}$$

This equation is only an approximation to the actual recording distance because of the errors introduced into the diffraction pattern by the Bessel function modulation of the sine term and the Airy pattern term. This theoretical error can be reduced to a certain extent by measuring ρ to the first minima of the diffraction pattern to reduce the effects of the modulation term and by keeping the recording plane at a large far-field distance which reduces the effects of the Airy term. From the theoretical data, the calculated Z from the first minimum of the intensity distribution, was as high as 21 per cent for small far-field numbers. At larger far-

field distances, where the Bessel function varies more slowly, the errors were below ten per cent. Figure 5 illustrates the theoretical error due to the approximations for a 320 μm diameter particle. Measurements of ρ were taken from the computer data of the particle and used in Equation 21 to calculate the recording distance. As the far-field distance increases the calculated recording distance is seen to approach the actual distance and become larger.

Calculating Particle Diameter

The particle diameter is found from the diffraction pattern by locating the zeroes of the Bessel function. Solving Equation 18 for a yields for the particle radius

$$a \doteq 3.86 \frac{Z}{\rho} \times 10^{-7} \text{ meters} \qquad (22)$$

To find the radius from zeros other than the first, the value of the desired zero is equated to the Bessel function argument following a development analogous to Equation 17. This equation is exact since when $J_1\left(\frac{ka\rho}{Z}\right) = 0$, all terms in the intensity distribution go to zero except the constant background term. The experimental error is in determining the exact location of the Airy minimum on the diffraction pattern.

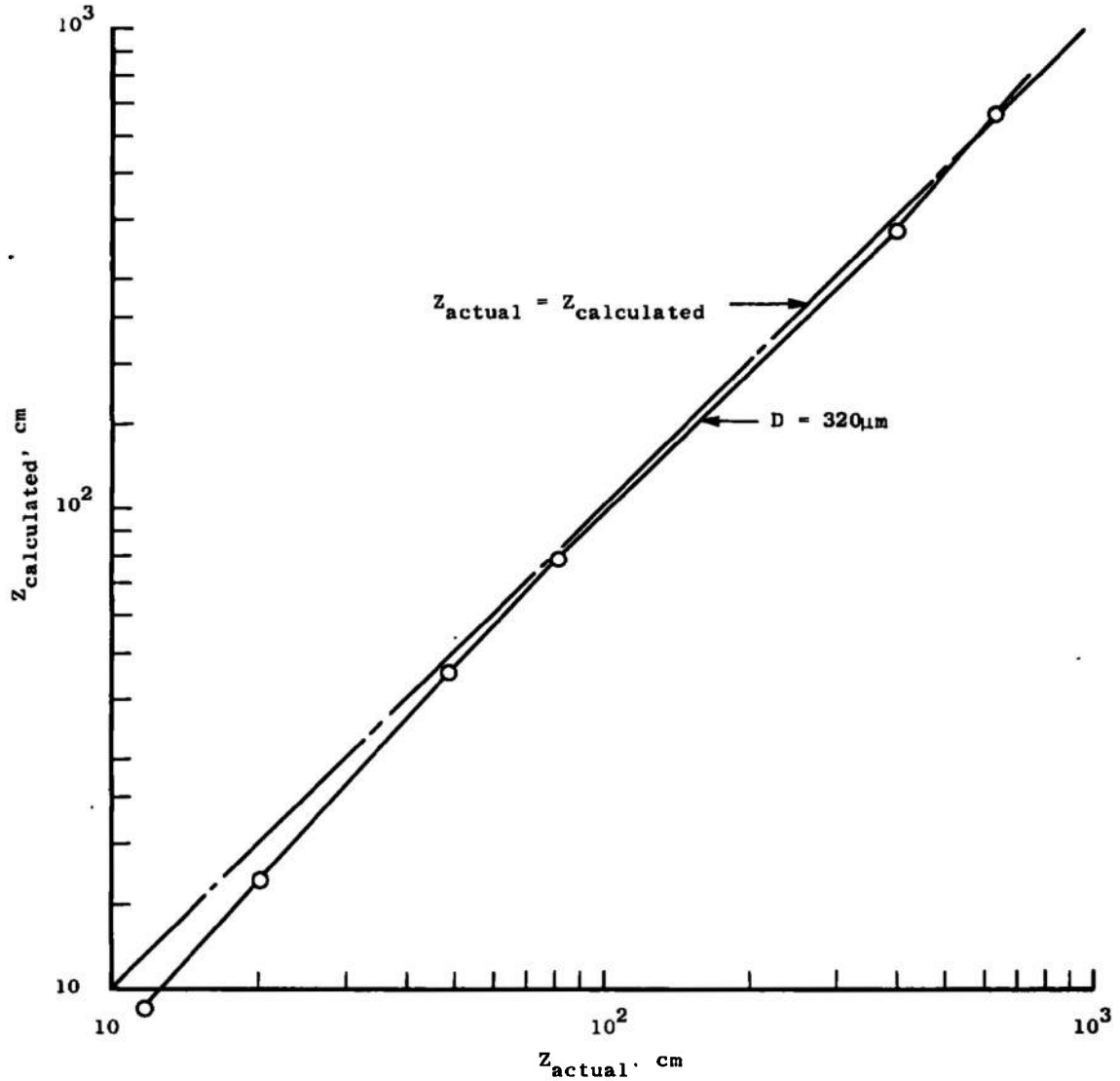

Fig. 5 Approximation error in the recording distance calculation

2.4 EXPERIMENTAL RESULTS

General Experimental Considerations

The experimental arrangement for recording the diffraction patterns of opaque particles is shown in Figure 6. A Helium-Neon laser was used as the light source with a pinhole-collimator to spatially filter and expand the beam to a 2-inch diameter. The spatial filter removes unwanted light from the laser beam, improving the spatial coherence. The laser operated with zero to thirty milliwatts of power with $\lambda = 0.6328$ μm. The particle field was composed of a random distribution of black paint particles ranging from 85 μm to 400 μm in diameter on an eight-inch thick plexiglass plate. The particles had good opacity as well as a fair degree of circularity. These characteristics as well as size determinations were made with a microscope. SO-243 sheet film was used to record the diffraction patterns because of its fine granularity and consequent high resolution, which helps to reduce the noise in the densitometer traces.

The laser, particle field and recording plane (a lensless 4 x 5 press camera) were mounted on an optical bench. A light intensity of $0.05 \frac{mw}{cm^2}$ illuminated the particle field, and an exposure time of 0.025 seconds was used to properly expose the film. The negative was developed in Kodak D-19 solution for three minutes and placed in the stop bath and fixer for 30 seconds and 1.5 minutes, respectively.

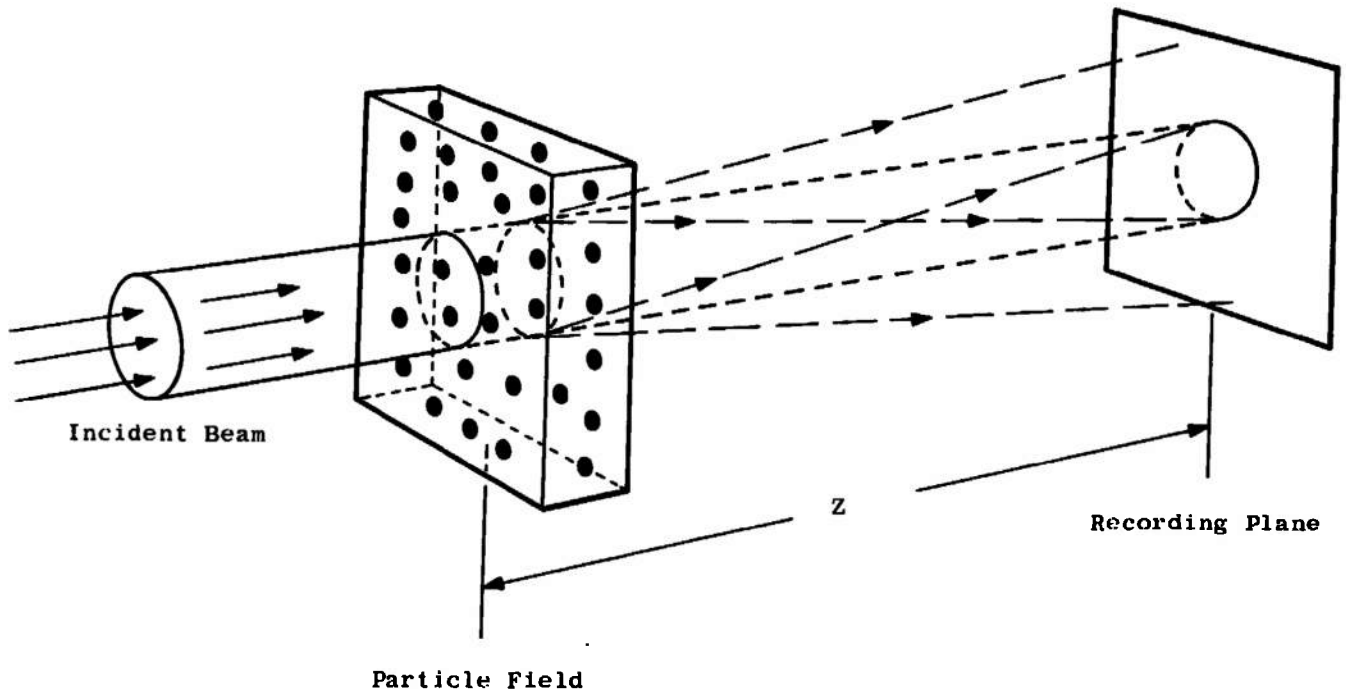

Fig. 6 Schematic arrangement for recording Fraunhofer diffraction patterns

Diffraction patterns recorded 15 cm from the paint particle are shown in Figure 7. Particle sizes are shown near a few of the patterns. The fainter diffraction rings seen scattered throughout the figure are from dirt particles on the plexiglass. Interference between light reflected from the two faces of the plate caused the straight-line diagonal fringes. Edge effects of the limiting aperture are also seen on the right.

The effects of increasing the far-field distance from a two-dimensional field are shown by the Fraunhofer diffraction patterns in Figure 8. The particle field of dust and paint particles was recorded at Z = 10, 20, 40 and 80 cm. Particle diameters representative of the field are shown near their patterns in Figure 8a, with the 230 μm particle indicated in Figure 8b, Figure 8c, and Figure 8d.

The variations of intensity of both the 280 μm and 130 x 150 μm particles in Figure 7 were recorded by a Jarrell-Ash photodensitometer. The traces are shown in Figures 9 and 10 respectively along with the theoretical curves of the particles. The traces were made along the line passing through the center of each diffraction pattern parallel to the background fringes to reduce extraneous noise from these fringes. Figure 11 shows the densitometer trace and the theoretical curve of the 210 μm particle in Figure 8 recorded 10 cm from the particle. The recording

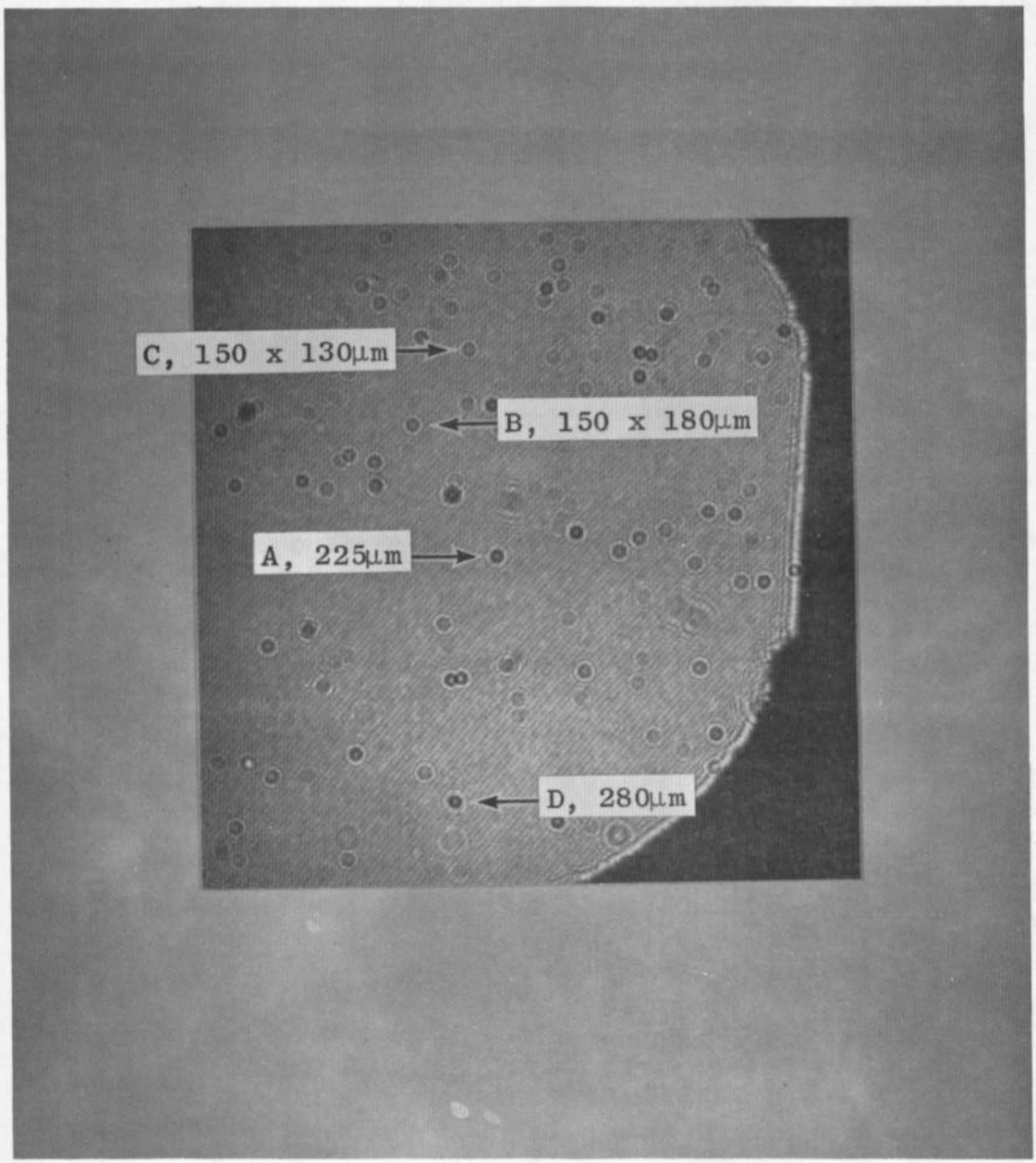

Fig. 7 Fraunhafer diffraction patterns of black paint particles recarded at Z = 15 cm on SO-243 film, λ = 6328 Å

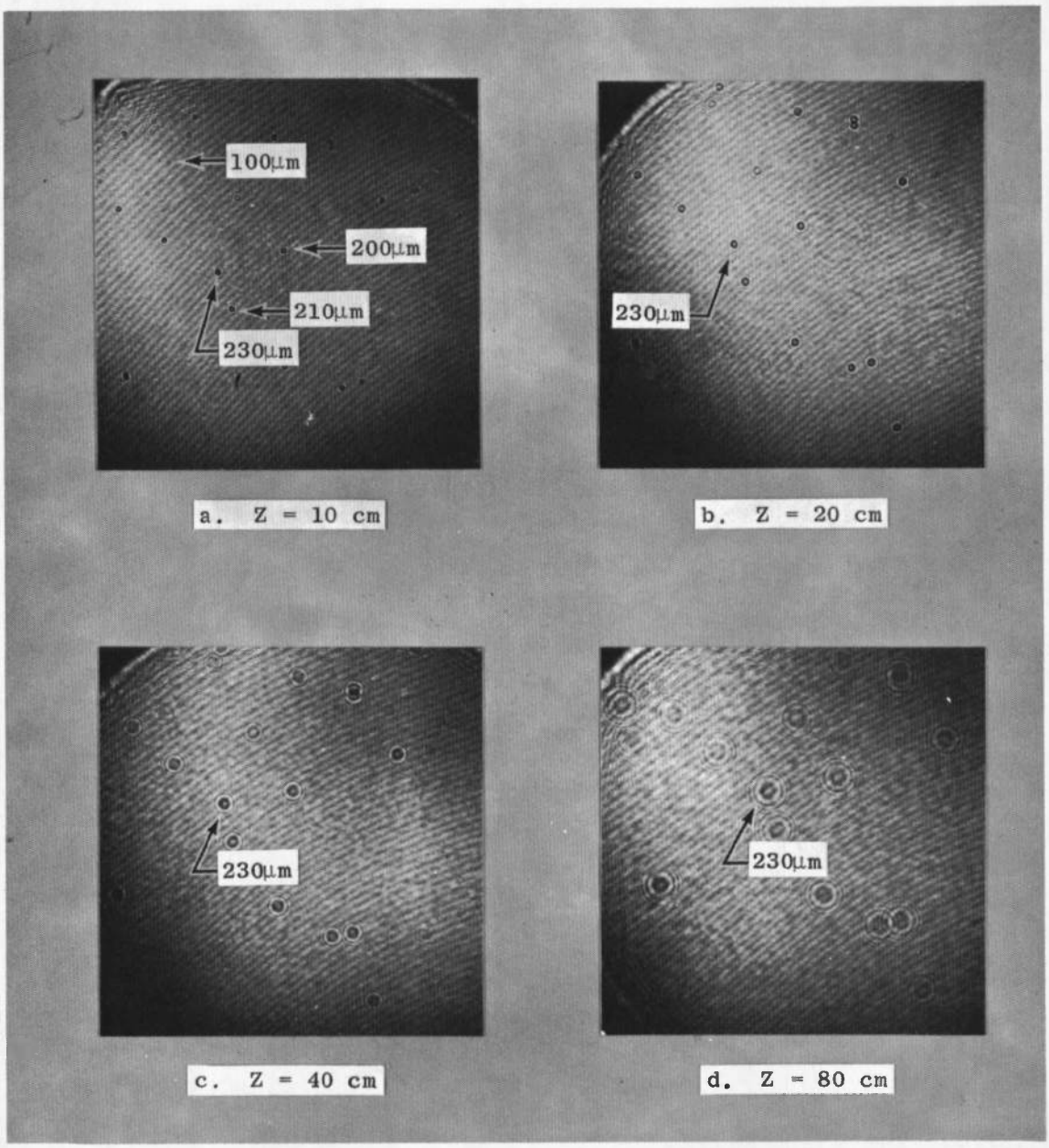

Fig. 8 Fraunhofer diffraction patterns of a two-dimensional particle field

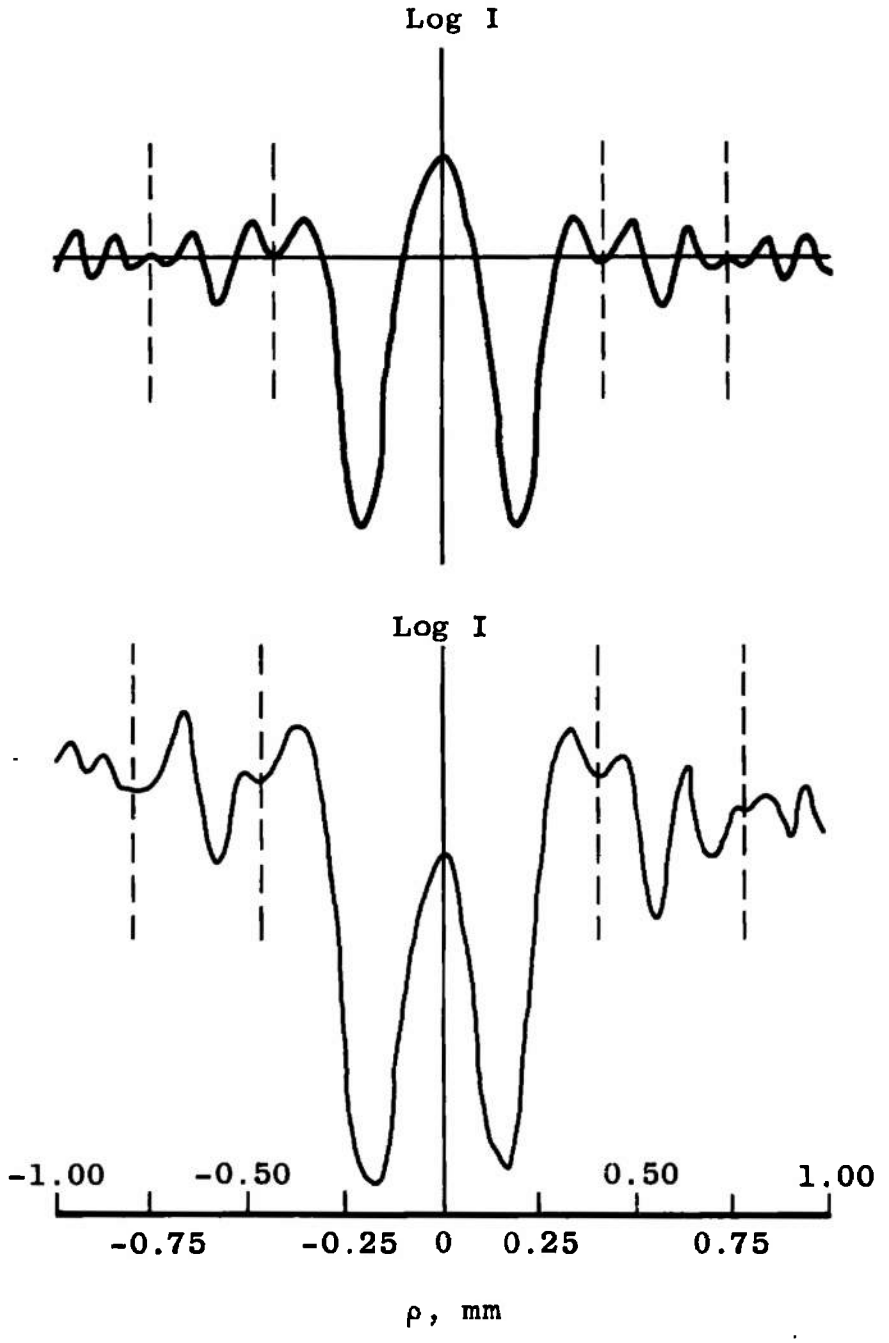

Fig. 9 Theoretical and experimental intensity curves of a 280 μm diameter particle recorded at Z = 15 cm with λ = 6328 Å

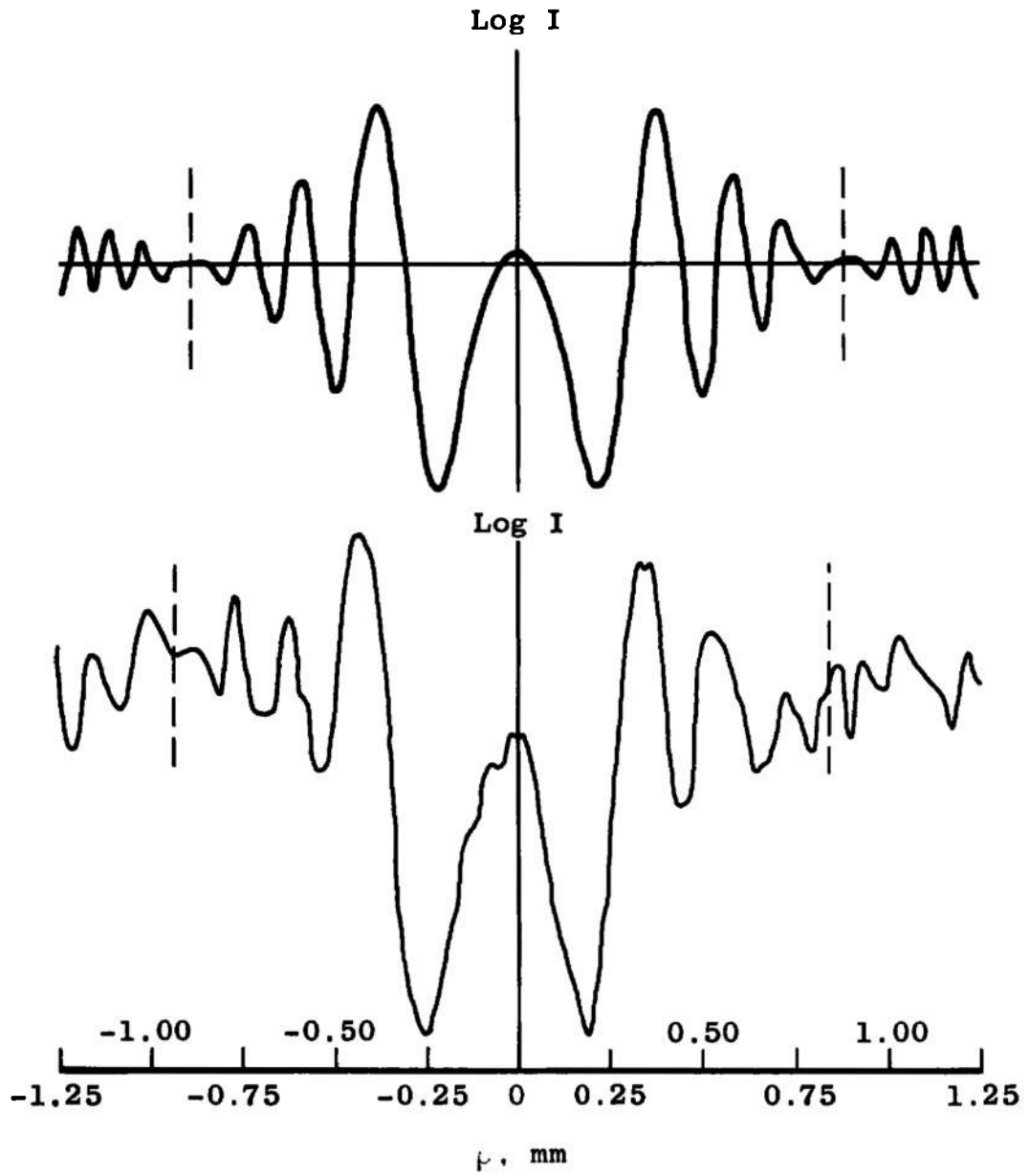

Fig. 10 Theoretical and experimental intensity curves of a 130 x 150 μm particle recorded at Z = 15 cm with λ = 6328 Å

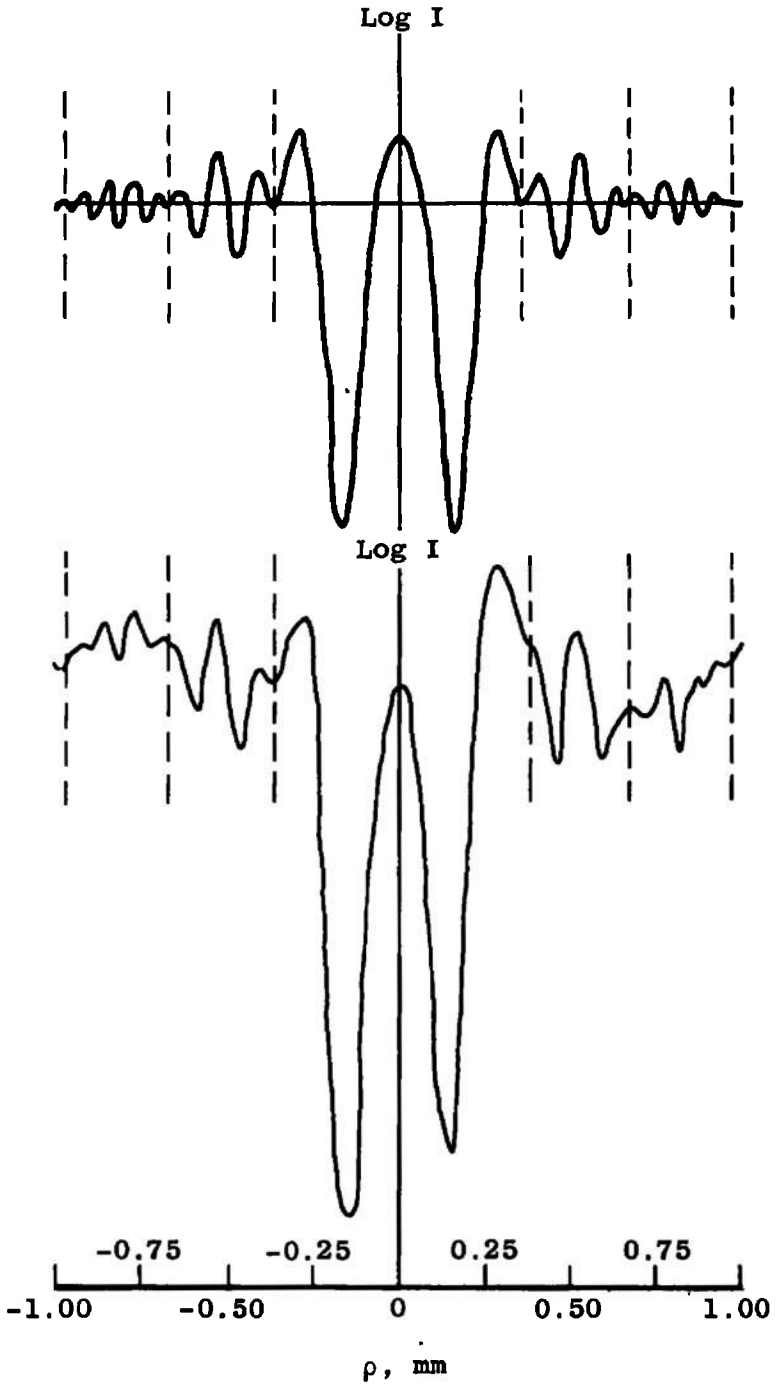

Fig. 11 Theoreticol and experimental intensity curves of a 210 μm diameter particle recorded at Z = 10 cm with λ = 6328 Å

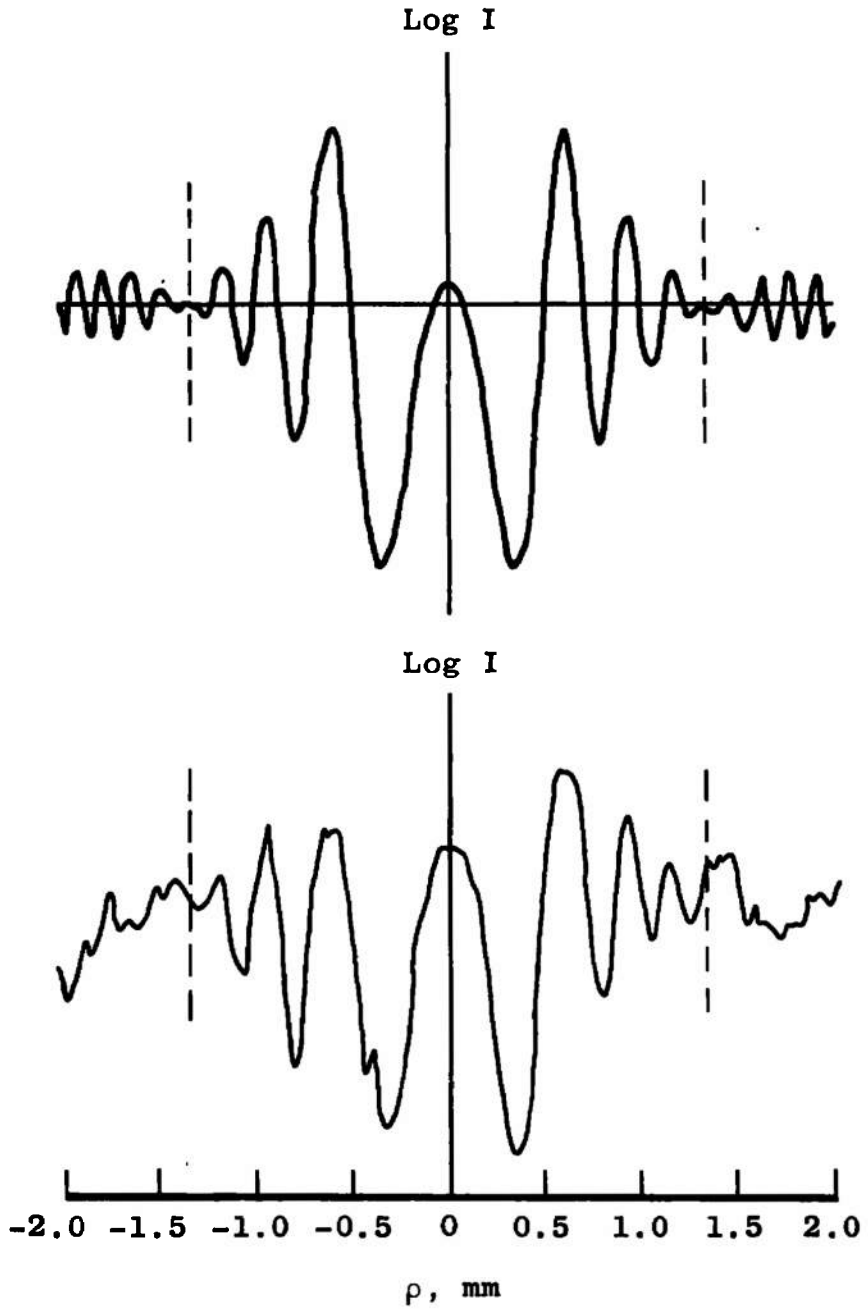

Fig. 12 Theoretical and experimental intensity curves of a 230 μm diameter particle recorded at Z = 40 cm with λ = 6328 Å

plane was 1.4 far-fields from the particle. The densitometer trace and theoretical curve of the diffraction pattern of a 230 μm particle recorded at 5.6 far-fields is shown in Figure 12. The data are from Figure 8, page 25, where Z = 40 cm. This curve represents the largest far-field distance the diffraction patterns could be recorded from the particles without the noise from the film producing extraneous intensity variations.

Experimental Recording Distance and Particle Size Calculations

The recording distances calculated from the first minimum of the densitometer traces in Figure 9, page 26, Figure 10, page 27, Figure 11, page 28, and Figure 12 are given in Table I, along with the known distances. This data verifies the statement made earlier in the recording distance calculation section that the smaller theoretical error occurs at the larger far-field distance.

Besides this inherent approximation error, error is also introduced into the experimental data by the densitometer and film. It is possible for the distance of travel of the chart recorder connected to the densitometer to be different from that of the densitometer slit across the film, due to changes in the motor speeds, or film slipping on the pressure plates. Care was taken to keep this error to a minimum. Another source of error lies in measuring the

TABLE I
EXPERIMENTALLY MEASURED AND CALCULATED RECORDING DISTANCES AND PARTICLE DIAMETERS

Figure No.	Far Field No.	Recording Distance, cm		Particle Diameter, μm	
		Measured	Calculated	Measured	Calculated
9	1.2	15	10.2	280	276
10	5.5	15	15.7	150 x 130	130.5
11	1.4	10	7.59	210	210
12	4.8	40	36.6	230	220

distance ρ on the densitometer traces. Any small error in measurement due to approximating the intensity peak is magnified in the recording distance calculation. This error was not considered in this investigation because of the seemingly well defined peaks in the data. The diffraction pattern recorded at the smallest far-field number (Figure 9, page 26) gives a 32 per cent overall error for the recording distance, while the recording distance calculated from the largest far-field number data (Figure 10, page 27) was 4.7 per cent too large. The distances to the first minima were measured from the densitometer traces by averaging over both sides of the patterns. Because of the lack of symmetry on each side this occasionally puts the center of the pattern slightly to the side of the central maximum.

Table I also compares the calculated and measured particle diameters for Figure 9, Figure 10, Figure 11, page 28, and Figure 12. The first Airy minimum indicated by the first dashed line from the center of each figure was used to calculate the particle diameters because, in most cases, it was difficult to distinguish the other minima from the system noise. The first minimum was easiest to detect on the densitometer traces taken of the diffraction patterns with low far-field numbers. The calculated diameters are in excellent agreement with the diameters measured with a 100 power microscope containing a reticle which divided the object field into

ten μm divisions. As in measuring the recording distance the average distance to the Airy minimum on each side of the densitometer traces was taken for the calculation.

2.5 CONCLUDING REMARKS

As is evident from the diffraction patterns in Figure 7, page 24, and Figure 8, page 25, the densitometer traces can only be taken where the particle density of the recorded volume was low. This is especially true for large far-field distances. Any intensity variations on the film from other diffraction patterns ruined the densitometer trace and made it difficult to locate the Airy minimum.

The range of particle radii that could be measured from a single negative was found to be limited to below an order of magnitude by the density range of the film. The density of the developed negative is related to the incident intensity by $D = \gamma \log(It + b)$ where γ is the slope of the straight line portion of the film's characteristic curve, t is the exposure time, and b is the film fog level constant. The background intensity sets the average density of the film. When the intensity of the diffraction pattern exceeds the gamma portion of the curve, the peaks will be recorded non-linearly. The gamma must then be decreased by reducing the developing time until the largest peak lies on the linear portion of the curve. On the other hand, if the intensity

varies over a small range there may not be enough light intensity to produce a recordable density variation on the film; therefore, the gamma should be increased so that a small intensity variation is amplified in the density. Figure 4, page 17, illustrated theoretically the difference in the intensity peaks for three sizes of particles at the same recording distance. The pattern of the smallest particle must be magnified considerably if the location of the Airy minimum is to be found.

The dimensions of non-circular particles cannot be accurately measured from their densitometer traces because of the assumed circular symmetry in Equation 16. Instead, an approximation to the particle size is found which lies between the maximum and minimum dimensions of the particle. This approximation will vary with the traversing angle the densitometer makes on the diffraction pattern. Figure 10, page 27, was taken of an oblong particle 130 x 150 μm. The calculation from the densitometer trace indicated a mean radius of 130.5 μm. This value of a was used in Equation 16 to obtain the theoretical curve in Figure 10.

SECTION III
FRAUNHOFER HOLOGRAMS

The amplitude and phase of the light diffracted or scattered from a particle field are uniquely related to the particle sizes and distances from the film plane. The phase information is lost in ordinary (incoherent) photographic processes since the film is sensitive only to the absolute value of the incident light: photographic film can only record intensities. When coherent light illuminates the field the diffracted light interferes with the undiffracted portion such that the phase difference between the two wavefronts modulates the resulting film plane intensity in a manner unique to the particles within the field. The amplitude and phase of the diffracted light is therefore recorded on the film as Fraunhofer diffraction patterns (for far-field recording) and constitute a hologram of the field. As will be seen, by illuminating the developed film with a wavefront similar to the one which illuminated the particle field, the total field can be reconstructed.

The reconstruction process forms two images, real and virtual, which lie on opposite sides of the hologram. The virtual image of the field lies between the hologram and the light source as shown in Figure 13 and is viewed by looking through the film. Because the reference beam was "in-line"

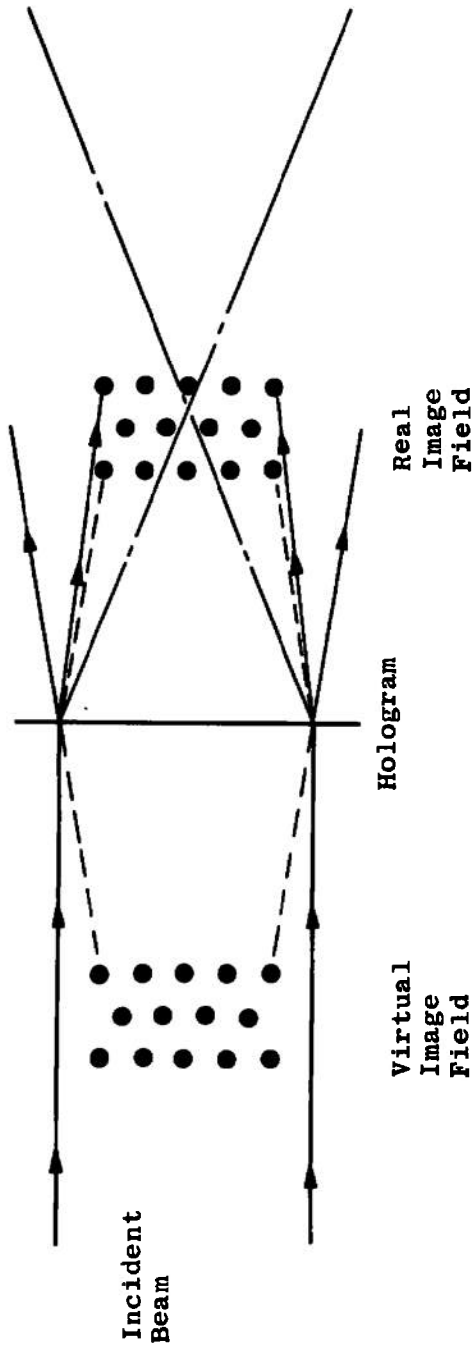

Fig. 13 Reconstructed image fields from a Fraunhofer hologram

with the object field, this image is centered within the reconstructing beam and is inconvenient to observe. The real image lies behind the hologram and reconstructs the object field without the aid of any auxiliary lenses.

In order to understand how the real and virtual images of the Fraunhofer hologram are formed from the diffraction patterns, it is necessary to observe the effects of the hologram on the incident illumination. This will be done in general terms and the results related to the results obtained in Section II, Equation 16.

3.1 THEORETICAL ANALYSIS

The film records two wavefronts from the object plane. One wavefront is due entirely to the background illumination and the other is produced by the object. These add coherently in the film plane to produce an optical disturbance $U(\bar{\rho})$ given by

$$U(\bar{\rho}) = A_1 e^{i\varphi 1} + A_2 e^{i\varphi 2} \tag{23}$$

where A_1 and A_2 are the magnitudes of the reference and object wavefronts, and φ_1 and φ_2, their respective phases. The intensity recorded by the film is

$$I = |U(\bar{\rho})|^2 = A_1^2 + A_2^2 + A_1 A_2 e^{i(\varphi_1 - \varphi_2)} + A_1 A_2 e^{-i(\varphi_1 - \varphi_2)} \tag{24}$$

This expression will be noted as being similar to Equation 13

in Section II, where the object disturbance was expressed as its Fourier transform.

The amplitude transmittance of the developed negative is related to the intensity by

$$T(\rho) \propto [It]^{-\gamma/2} \tag{25}$$

where γ is the slope of the straight-line portion of the D-log E curve of the film. Substituting Equation 24 for the intensity of this Equation gives the amplitude transmission of the hologram. Assuming the background is greater than the diffracted light, this Equation can be expanded in a binomial series to give

$$T(\rho) = H\left(A_1^2 - \frac{\gamma}{2} A_2^2 - \frac{\gamma}{2} A_1 A_2 e^{i(\varphi_1 - \varphi_2)} - \frac{\gamma}{2} A_1 A_2 e^{-i(\varphi_1 - \varphi_2)}\right) \tag{26}$$

where $H = A^{-(\gamma+2)} t^{-\gamma/2}$ and is a constant. When the film is illuminated with an incident beam, the light is attenuated and diffracted according to this equation. The first two terms serve only to attenuate the beam. The first term represents a constant attenuation, and the second term attenuates it according to the recorded amplitude variation of the diffracted wave.

The third and fourth terms contain the information necessary to reconstruct the real and virtual images of the particle field, respectively. These terms diffract and

attenuate the light passing through the hologram in such a way that concave and convex wavefronts emerge from the hologram which contain the information necessary to form the two separate images. To understand how these wavefronts are formed in a Fraunhofer hologram, it is necessary to first look at the intensity distribution recorded in the film plane given by Equation 13 in Section II. When this Equation is substituted into the amplitude transmittance equation and expanded, the transmittance of the film becomes

$$T(\rho) = 1 - \frac{\gamma}{2} \frac{k^2}{r^2} [\tilde{D}(\rho)]^2 - \frac{\gamma}{2} \frac{ik}{r} \exp \frac{-ik|\bar{\rho}|^2}{2Z} \tilde{D}(\rho)$$

$$+ \frac{\gamma}{2} \frac{ik}{r} \exp \frac{ik|\rho|^2}{2Z} \tilde{D}(\rho) \qquad (27)$$

where the background intensity, A, and the total attenuation of the transmittance given by H in Equation 26 have been normalized. Again, the first two terms of the transmittance equation are constants and do nothing to form the real and virtual images. The third term diffracts the incident light and forms the real image. This can best be understood by recalling the effects a positive thin-lens has on a plane wave. By definition a lens is a device that converts a plane wavefront into a spherical wave of radius f. This is illustrated in Figure 14. The phase change in the spherical wavefront introduced by the lens is given by

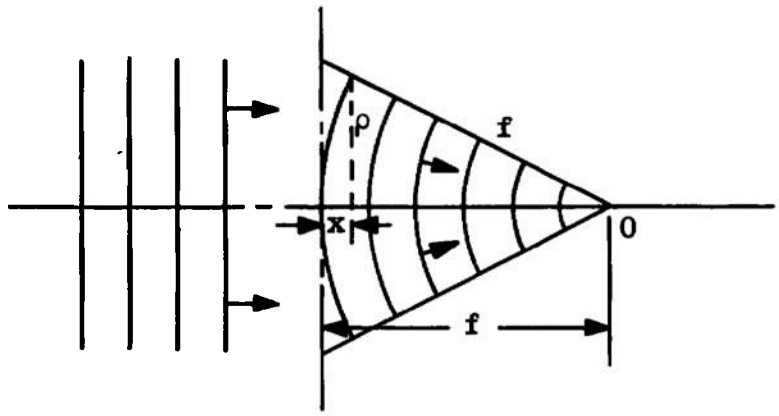

Fig. 14 Effects of a positive thin lens on a plane wave

$$\varphi = kx \tag{28}$$

From the right triangle in the Figure, the paraxial assumption that $x \ll \rho$ is made, so that the sagital approximation results for x, that is

$$x = \frac{|\rho|^2}{2f} \tag{29}$$

The phase change is therefore

$$\varphi = \frac{k|\overline{\rho}|^2}{2f} \tag{30}$$

From this it is seen that the exponential in the third term of Equation 27 will produce a positive lens-like phase shift in the incident beam, and like a lens, a Fourier transform of the term, $\tilde{D}(\rho)$, will occur at the "focal point" of the hologram forming the real image at Z. Likewise the fourth term represents a negative lens that has a virtual focal point. Thus, the virtual image is formed behind the hologram by this last term. The location of these images is shown in Figure 13, page 36.

The intensity distribution in the reconstructed real image plane has been derived to be (5)

$$I(\overline{\alpha}) = 1 + \gamma D(\overline{\alpha}) \cos\left(\frac{k\alpha^2}{2Z}\right) + \frac{\gamma^2}{4}[D(\overline{\alpha})]^2 \tag{31}$$

where $\bar{\alpha}$ is the position vector in the image plane and the other terms were used earlier.

The first term is once again the normalized background. The second term contains the reconstructed image $D(\bar{\alpha})$ which is interlaced with slowly varying cosine fringes that do not degrade the image. The third term is the out-of-focus virtual image which causes most of the deterioration in Fresnel holograms but very little in Fraunhofer holograms.

3.2 EXPERIMENTAL DATA

The Fraunhofer holograms were recorded in the same manner as was the experimental data of Section II. The particle field was illuminated with plane waves of quasi-monochromatic light where λ = 6328 Å and the far-field diffraction patterns were recorded on SO-243 film. Upon illuminating the developed hologram with another plane wave, the reconstructed particle field was imaged and recorded on Polaroid film. Figure 15 shows an opaque paint particle field and below it, its reconstructed real image. The negative images of the opaque particles are characteristic of the in-line holographic technique. The particle field was reconstructed 15 cm from the hologram, the same distance the hologram was recorded. The photographed field is shown magnified four times actual size and the reconstructed field is approximately five times where magnification was due to the camera lens. The virtual image of the field could be seen by

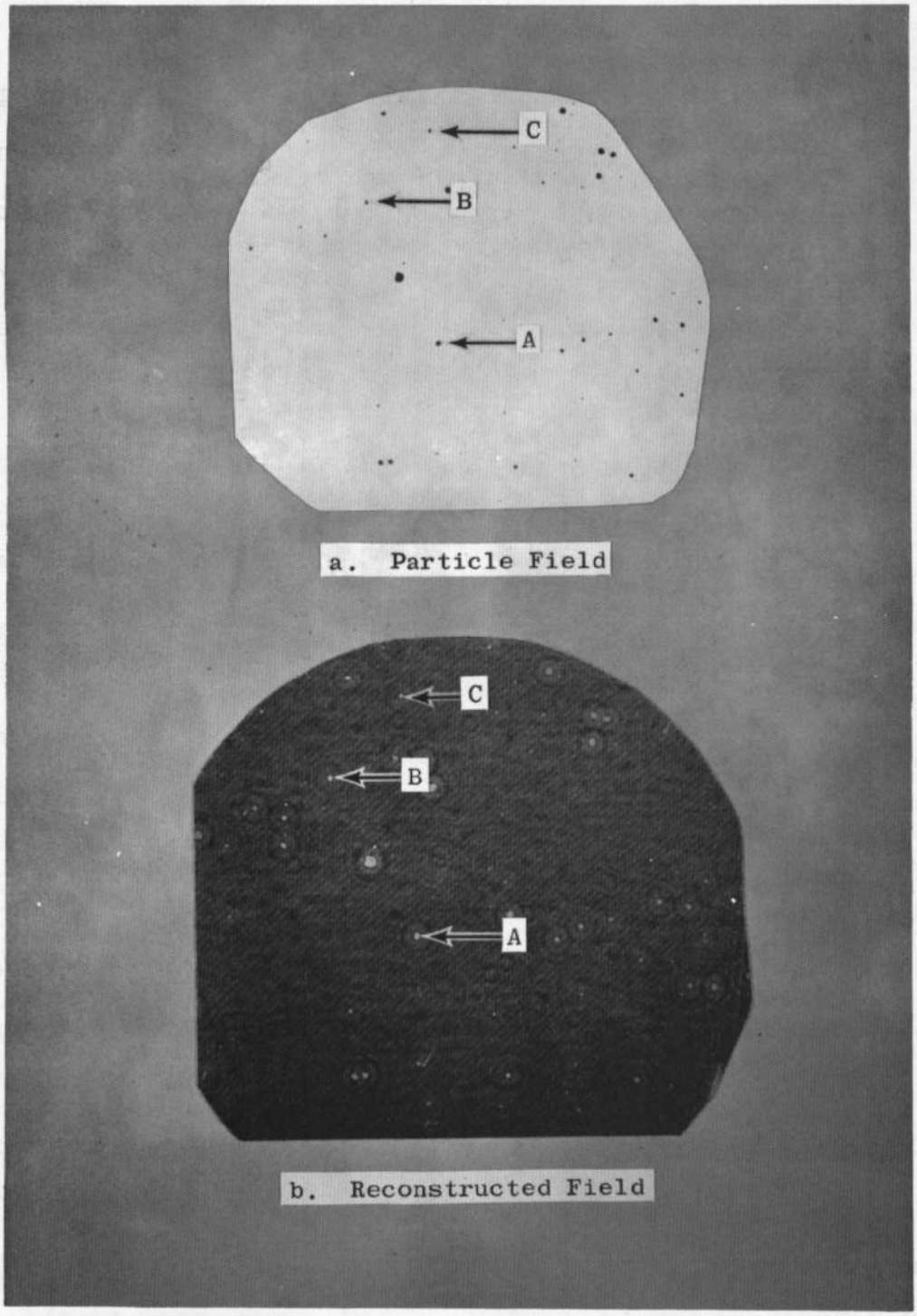

Fig. 15 Opaque two-dimensional particle field and the reconstructed real image from a Fraunhofer hologram

looking directly into the hologram when the power of the illuminating beam was sufficiently lowered so as not to harm the eyes. There was no recognizable difference between the real and virtual images when they were imaged onto the viewing screen with a lens. In fact, one was always being confused with the other since both contain exactly the same information, only each is located on a different side of the hologram.

Particles A, B, and C labeled on the photographed field and on the reconstructed image in Figure 15 are the same particles whose diffraction patterns are shown in Figure 7, page 24. Figure 7 is the positive of the hologram that was used to reconstruct the field. The densitometer trace of particle C was also shown in Section II in Figure 10, page 27.

To simulate a volume of particles two plexiglass plates with opaque paint particles on them were placed five cm apart with the first plate 18 cm from the recording plane containing SO-243 film. Reconstructed images of these plates were recorded in planes separated by five cm and are shown in Figure 16. The images are magnified nine times. The large paint particles are approximately 220 μm in diameter and the small dust particles about 55 μm. Arrows indicate a few of the particles that are in focus in each picture. The loop in Figure 16a was part of a small thread from a cleaning tissue. The thread is about 85 μm in diameter. The particle images

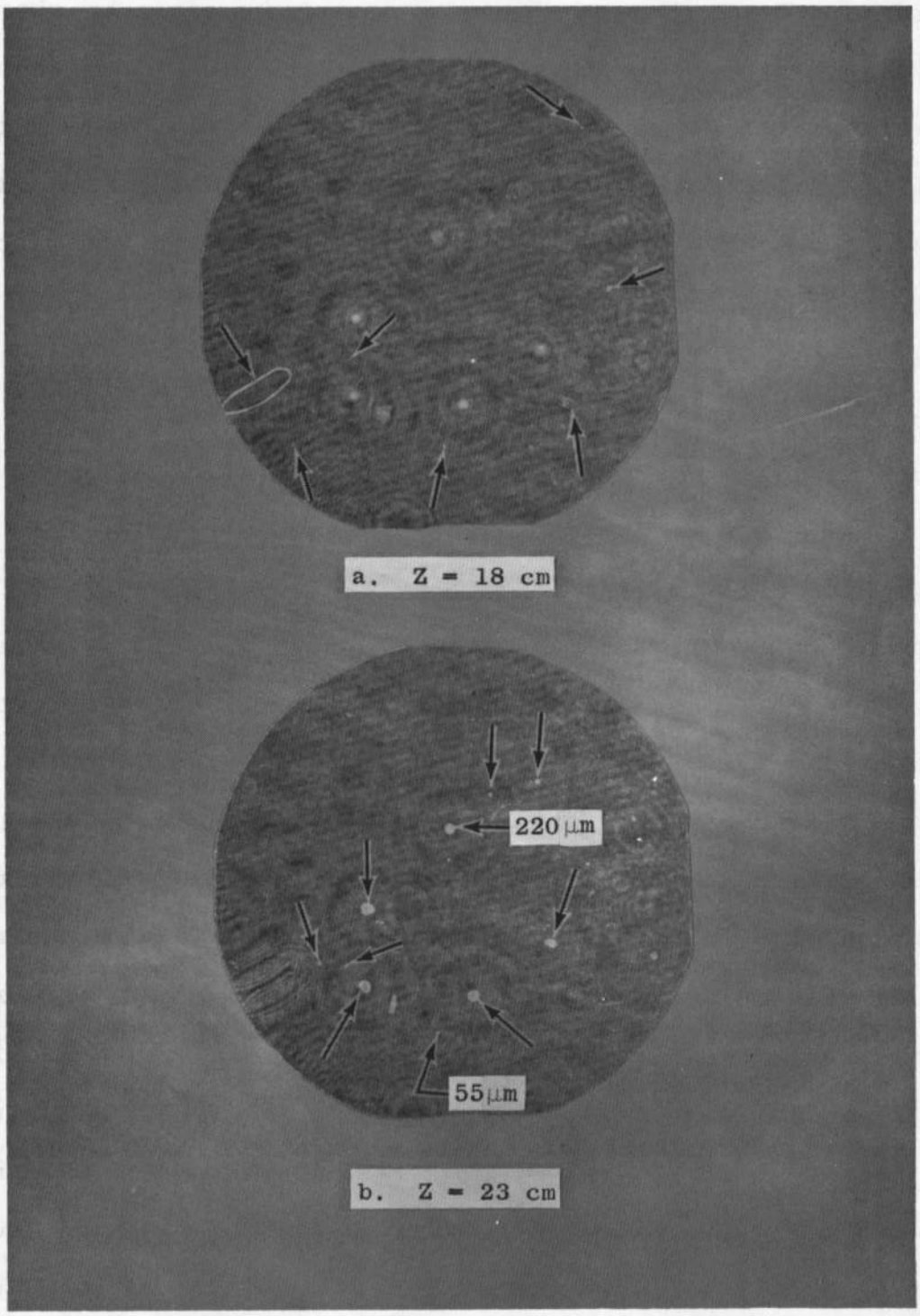

Fig. 16 Reconstructed real images from a Fraunhofer hologram of two planes separated by 5 cm

in these pictures are sharp and clear so that measurements can be taken of them. Densitometer traces of these particles were impossible to obtain because of the particle density.

A volume of opaque paint particles from the aerosol were photographically stopped in space and the hologram recorded on SO-243 film. The volume of particles was generated by a spray paint can centered approximately 39 cm from the recording plane. The schematic arrangement is shown in Figure 17. The reconstructed real images are shown magnified nine times in Figure 18. Five planes are shown in this figure; each plane is separated by one cm with the first plane 37 cm from the film. The volume extended five cm in the Z direction and the width of the reconstructed area was seven mm. Particle motion was stopped by a fast shutter with a speed of 10^{-3} seconds. The particle diameters measured from this figure are approximately 81 μm. A few of the particles in focus are indicated by arrows in each figure.

3.3 FRAUNHOFER HOLOGRAM LIMITATIONS

Particle Size Limits

The limit on the minimum size of particles that can be reconstructed from a Fraunhofer hologram is set by the far-field restrictions made in the derivation of the intensity from the diffraction integral which includes the condition that the dimensions of the diffracting particle be

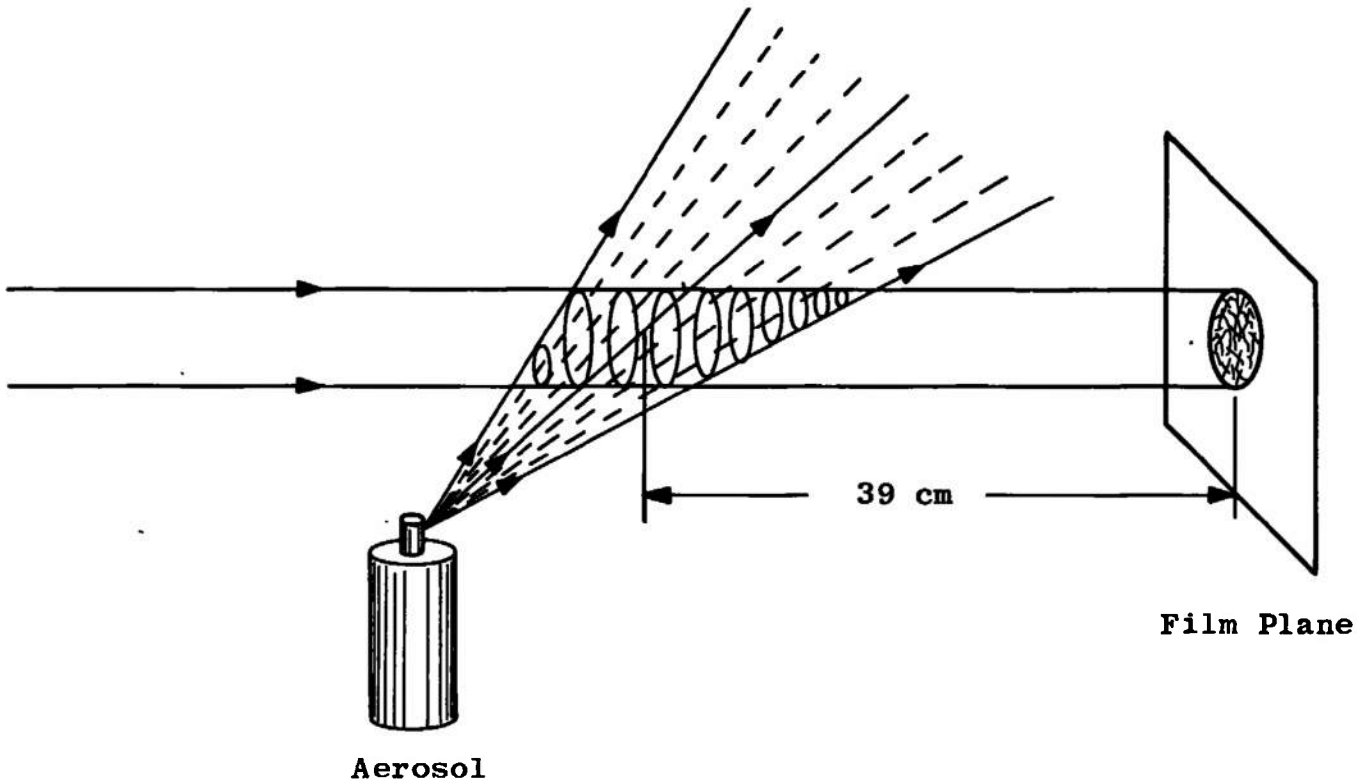

Fig. 17 Schematic arrangement for recording an in-line Fraunhofer hologram of opaque paint particles

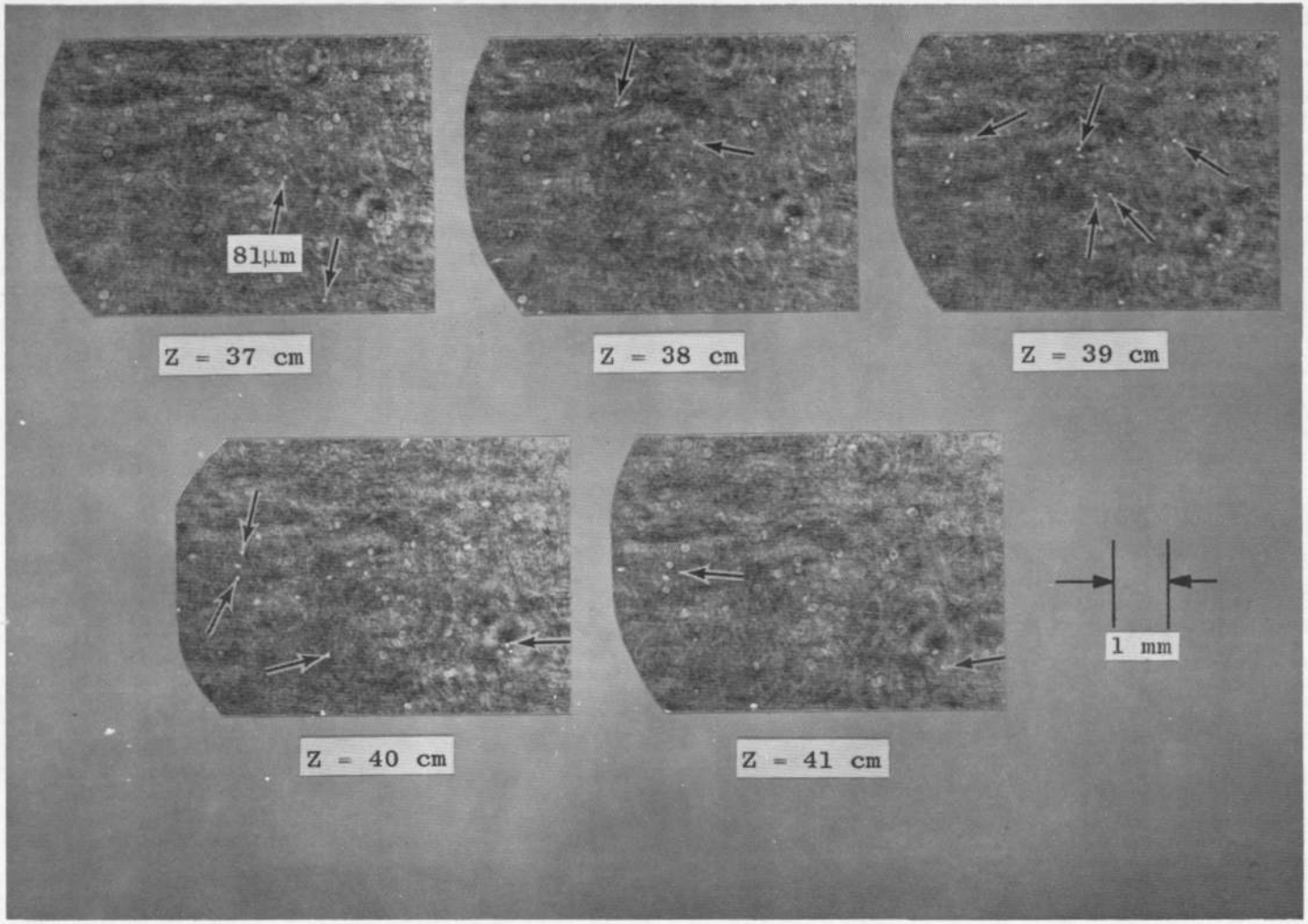

Fig. 18 Reconstructed image planes from a Fraunhofer hologram of a spray paint volume

larger than the wavelength of the illuminating radiation. For a He-Ne laser which emits a wavelength of 6328 Å, this limit is about one μm. The smallest particles recorded in this study have been about 25 μm. Any particles below this limit were difficult to observe. As will be shown in the next chapter on magnification, magnifying a particle in the recording or reconstruction process increases the reconstructing distance directly as the magnification. Therefore, any large magnification of a small object tends to make the reconstruction distance uncomfortably long.

The maximum particle size that can be recorded in a Fraunhofer hologram is determined by the far-field or Fraunhofer condition given by Equation 2, that is

$$(2a)^2 \leq Z\lambda$$

Holograms taken closer than this distance are Fresnel holograms and the reconstructed image is deteriorated by the conjugate image. For a particle one mm in diameter, the Fraunhofer recording distance must be over one meter long; therefore, for large particles, Fraunhofer holograms are difficult to take.

Recording Distances

Theoretically, there is no limit on how far the particle can be from the recording plane, since its diffraction

pattern is Fraunhofer at infinity. From a practical standpoint, however, the recording distance is limited by the response of the film to the diffracted light. As the recording plane moves farther from the particle, less diffracted light will strike the film, resulting in slowly varying low-contrast fringe patterns which are severely limited by system noise. The signal-to-noise ratio of the film thus limits the length of the recording distance from the particle. In terms of far-field number it has been found (10) that for clean reconstructions

$$N \leq 100$$

Recording at this large far-field distance where the fringe contrast is low results in poor contrast between the images and the background. Since the particle information is spread out over an even larger area of the film than the sinusoidal interference frequency the resolution of the image is poorer.

In Figure 19, this far-field criterion is plotted for particle radii from one to 10^3 μm and recording distances from 0.01 to 10 meters. Any recording situation lying above this curve will result in images of poor contrast and resolution. The minimum recording distance criterion, N = 1, for Fraunhofer holograms is also plotted in the Figure. These two curves define the range where the particle field will be reconstructed cleanly.

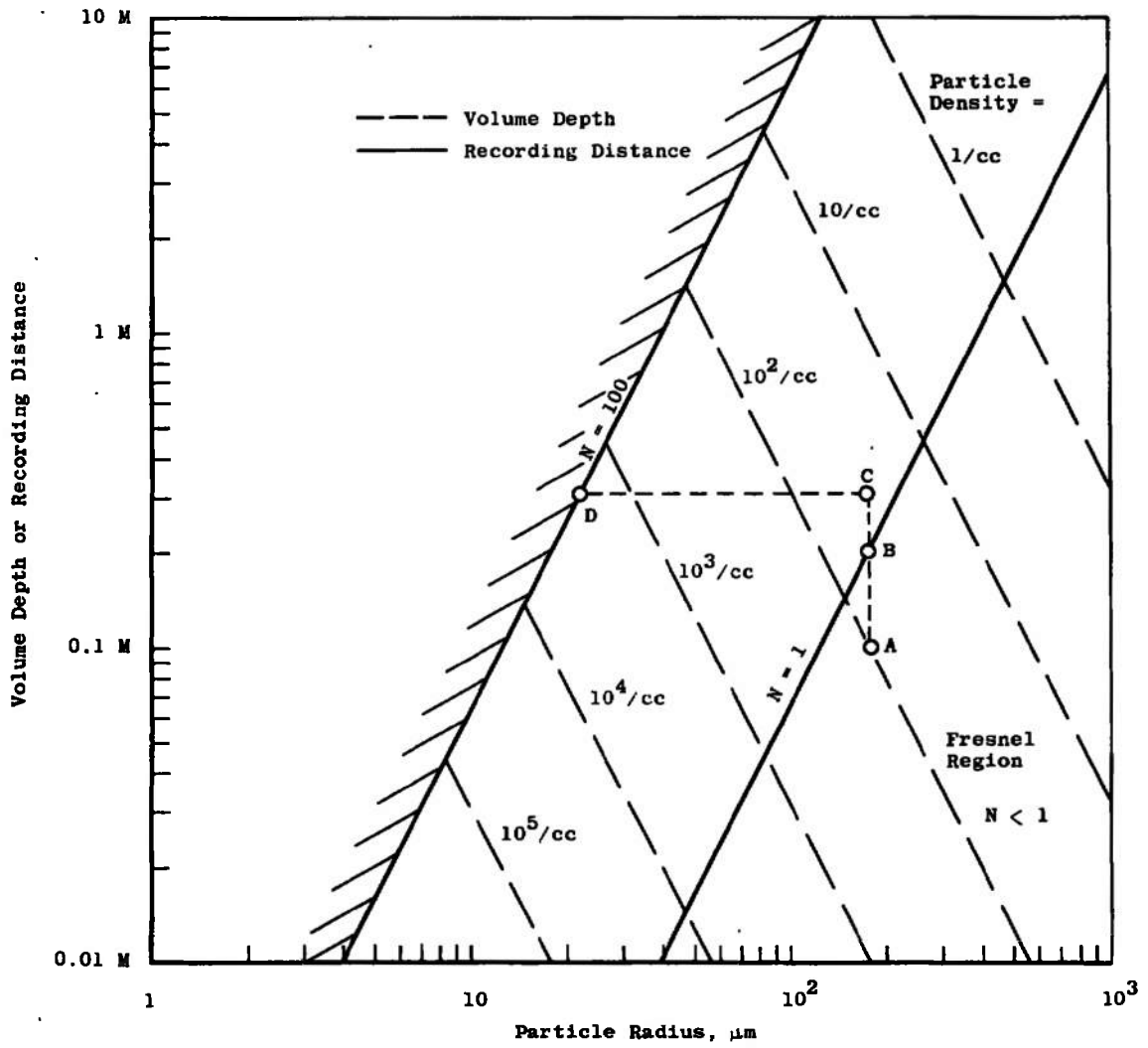

Fig. 19 Dependence of recording distance and volume depth on particle size and density for clean reconstructions from Fraunhofer holograms

Depth of Field

The field depth was found to be limited by the particle density as well as the recording distance. The particle density limits the volume size since all of the information in the three-dimensional volume must be recorded on a two-dimensional plane. Too large a density keeps the information from the particle farthest away from reaching the recording plane. Enough background light must also get through the volume to record the hologram. This background light attenuation was used to obtain a criterion for the density and volume size as follows.

The intensity of the undiffracted light, I, passing through the volume is given by Beer's law (14).

$$I = I_o e^{-z/L} \tag{32}$$

where I_o is the illuminating intensity, z is the volume depth, and L may be regarded as the mean free path of the light. For particles of cross-sectional area A with density n, the mean free path is

$$L = \frac{1}{An} \tag{33}$$

where it has been assumed that the total scattering cross-section of pertinence is equal to the geometrical cross-

sectional area (11). Assuming that the minimum background light necessary to record a hologram is $I_o e^{-1}$, then the volume depth must be less than the mean free path, that is,

$$z \leq \frac{1}{An} \tag{34}$$

Therefore, as the particle size or density decreases, the volume may become larger. How large the volume can become is determined by the maximum Z-dimension of the volume from the recording plane and the smallest particle contained within it. The recording plane must be less than 100 far-field distances from the particle to maintain clean reconstructions.

Figure 19, page 51, illustrates the restrictions made on the width of the volume by its particle density. The constant density curves plotted from the equality in Equation 34 are shown as dashed lines. The density range is from one to 10^5 cm^{-3}. Given a constant density and particle size, the depth of field of the volume can be found. The lines of constant density were extended into the Fresnel region so that the recording plane distance from a given volume could be calculated without having the larger particles recorded in the Fresnel region. If a volume is 10 cm deep and has a particle density of 10^2 cm^{-3} then the particles must have radii less than 178 μm or the medium will be too dense. The volume must also be at least 20.5 cm from the recording plane. This

data was obtained by finding the intersection of the 10 cm volume depth with the density (Point A on graph) and moving this point vertically upward into the Fraunhofer region (Point B). The smallest particle size that will give clean reconstructions is found by assuming the worse case condition, that is, the particle is located in the volume at the maximum recording distance from the film plane. Therefore, the volume depth is added to the minimum recording distance (Point C), and this total distance intersects the N = 100 curve at Point D. The smallest particles that would reconstruct cleanly in this example would be 30.5 cm from the recording plane and must have radii of at least 22 μm. Figure 19, page 51, may then be used for engineering design when two of the parameters are known (or assumed).

Out-of-Focus Images

Trouble in locating the position of the particles in the reconstructed volume came about from out-of-focus particle images in adjacent planes. It was found that the point of exact focus for the larger particles could not be determined as easily as for the small particles because of the intensity of the out-of-focus images. This effect is seen in Figure 16a, page 45, where the image of the large particles in focus in Figure 16b, five cm away, are still evident. The images of any small particles present in-line with these out-of-focus images would be difficult to find. For a smaller

increment of the photographed planes it was difficult to determine in which plane the larger particles were in focus. It is seen in the spray paint volume in Figure 18, page 48, that even for small particles, if an individual plane is studied in the middle of the volume where the density is high, the out-of-focus and in-focus particles are difficult to distinguish. This gave an accuracy of approximately five mm for Z. Particles in focus were found by observing their images in each photographed plane and finding where they were sharp and bright.

Because of the bright out-of-focus images for the larger particles, planes within the reconstructed volume could be focused upon in a precise manner by observing when the small particles ($< 100\mu$) appeared on the recording plane. The two-dimensional fields in Figure 15, page 43, and Figure 16, page 45, were assumed to be in focus when the small threads in each field were sharply defined in the reconstruction plane.

SECTION IV
MAGNIFICATION OF THE PARTICLE FIELD

4.1 INTRODUCTION

In order to accurately measure the diameter of the particles in the recorded volume from the reconstructed image, it is necessary to magnify the particle field. This is done by using spherical waves or lenses in either the recording or reconstruction steps, or both. Magnification with spherical waves is given as (10)

$$m_s = \left[\frac{R_1}{R_1 + Z} - \frac{k_2 Z}{k_1 R_2} \right]^{-1} \tag{35}$$

where R_1, Z and k_1 are the distance from the point source to the object field, the recording distance, and the wave vector of the recording step, respectively, and R_2, Z_2 and k_2 are the same parameters in the reconstruction. These are shown schematically in Figure 20. When a lens is used to magnify the particle field, the magnification is found from the thin-lens equation

$$m_\ell = -\frac{\ell'}{\ell} = -\frac{f}{\ell - f} = -\frac{\ell' - f}{f} \tag{36}$$

where ℓ is the object distance and ℓ' is the distance of the

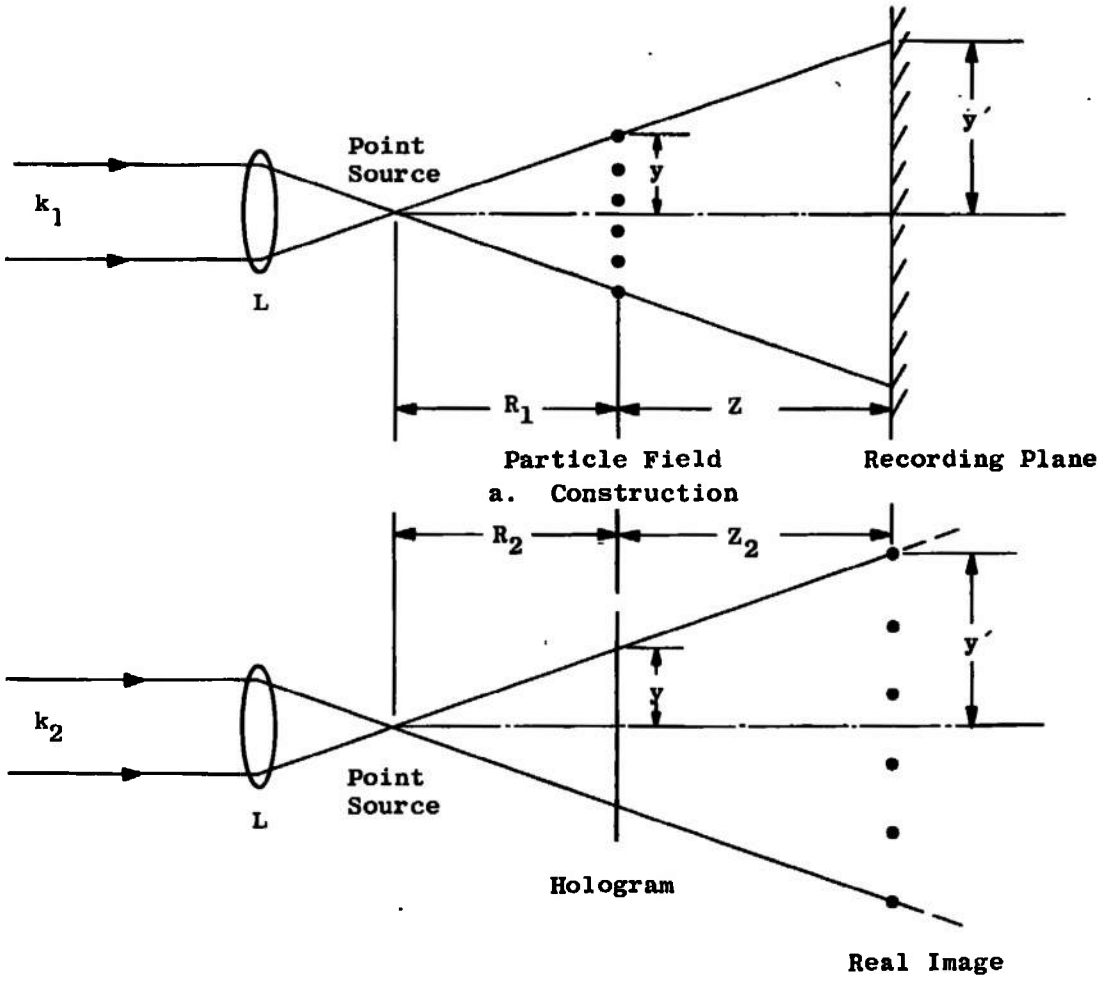

Fig. 20 Magnification of the particle field using spherical waves in recording and reconstruction

image from a lens of focal length f. The negative sign indicates the image is inverted.

The reconstruction distance Z_2 increases linearly with the system magnification and is given by (10)

$$m = \frac{\lambda_2 Z_2}{\lambda_1 Z} \tag{37}$$

Therefore, the advantages gained from magnifying the particle field are offset in the reconstruction by a longer image formation distance.

This equation cannot be applied to the case of plane wave recording and reconstruction in order to magnify the reconstructed volume with a longer wavelength source. It was found from the theory (10) that the condition necessary for bringing the images into focus reduces Equation 37 to unity. Only the position where the image is in focus will change with wavelength. This is understood by noting that the point of focus of a Fresnel lens is a function of wavelength. Therefore, because the object characteristics modulate the focusing (Fresnel lens) term in the intensity pattern, only the longitudinal position of the image changes. For spherical waves the magnification will change with wavelength as shown by Equation 35.

4.2 MAGNIFICATION IN THE RECORDING PROCESS

Spherical Waves

When spherical waves are used to magnify the particle field in the recording process, and the image is reconstructed with a plane wave, the magnification is given by Equation 35 when $R_2 = \infty$ as

$$m_s = 1 + \frac{Z}{R_1} \tag{38}$$

This result may also be obtained by observing in Figure 20a, page 57, that the linear magnification is

$$m_s = \frac{y'}{y} = \frac{R_1 + Z}{R_1} = 1 + \frac{Z}{R_1} \tag{39}$$

where the second equality follows from the similar triangles involved.

Figure 21 shows the Fraunhofer hologram and reconstructed image of a 200 μm particle field recorded with spherical waves and illuminated with a plane wave of λ = 6328 Å. The particle field was 20 cm from the focal point of the lens and 40 cm from the recording plane. Magnification was 3x. The image was reconstructed 114 cm from the hologram with collimated light. The recorded cross-sectional area of the volume is smaller than in the plane wave case

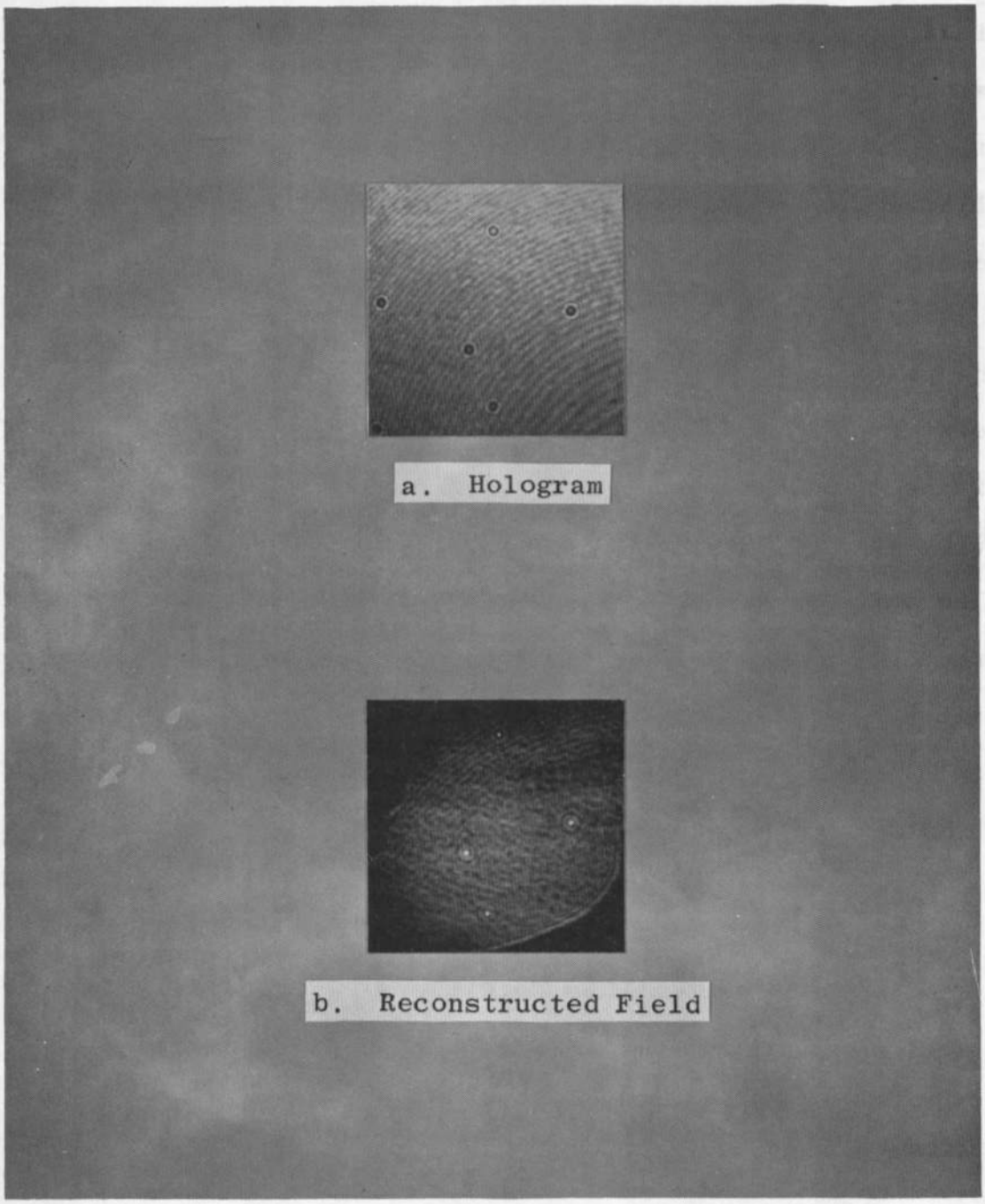

Fig. 21 Magnificotion of o plonor porticle field by sphericol wove recording of a Frounhofer hologram where m = 3x

because of the smaller illuminating area of the diverging light when the same film area is illuminated. Because of the magnification, the recorded diffraction patterns are three times larger than they would be in the case of plane wave illumination, thus allowing more particle information to be recorded on the film.

The focal point of the lens must be placed away from the particle field so that the Fraunhofer conditions for a point source given by Equation 1 are obeyed. The first condition limits the amount of magnification that can be introduced into the recording process since increasing Z and m_s also increases Z_2 directly, according to Equation 37. For a Fraunhofer hologram of a 200 μm particle magnified ten times with R_1 = 10 cm, (to keep the recording plane in the far-field), the reconstructed image is in focus nine meters from the hologram.

For a three-dimensional volume, each plane within the volume is magnified differently. This limits the spherical wave recording of Fraunhofer holograms to planar fields if different longitudinal magnifications cannot be tolerated.

Thin Lenses

A thin lens may also be placed between the particle field and recording plane to magnify the field. The lens images the optical disturbances in a plane removed from the particle field onto the recording plane at L as shown in

Figure 22. Therefore, the system magnification is due entirely to the lens and, according to Equation 36,

$$m_{\ell} = -\left(\frac{L - f}{f}\right) \tag{40}$$

The image is inverted and magnification is independent of the particle position, but the object plane of the lens must be in the far-field of the particles for Fraunhofer holograms.

The lens can also be thought of as operating on the particle field itself as shown in Figure 22b. The inverted image of the field at ℓ' is illuminated by spherical waves from the focal point of the lens. The system magnification is then the product of the lens magnification and the spherical wave magnification which is

$$m = -\frac{\ell'}{\ell}\left(1 \div \frac{Z}{R_1}\right) \tag{41}$$

Equation 40 can be subsequently derived from this equation by solving the thin-lens formula for ℓ and putting ℓ' in terms of the focal length and the radius of the spherical waves illuminating the image of the particle field.

The diffraction patterns and reconstructed images of an opaque particle field 14.7 cm from a 7 cm focal length lens are shown in Figure 23. The recording plane was 52 cm from the lens, yielding a magnification of 6.4. The image

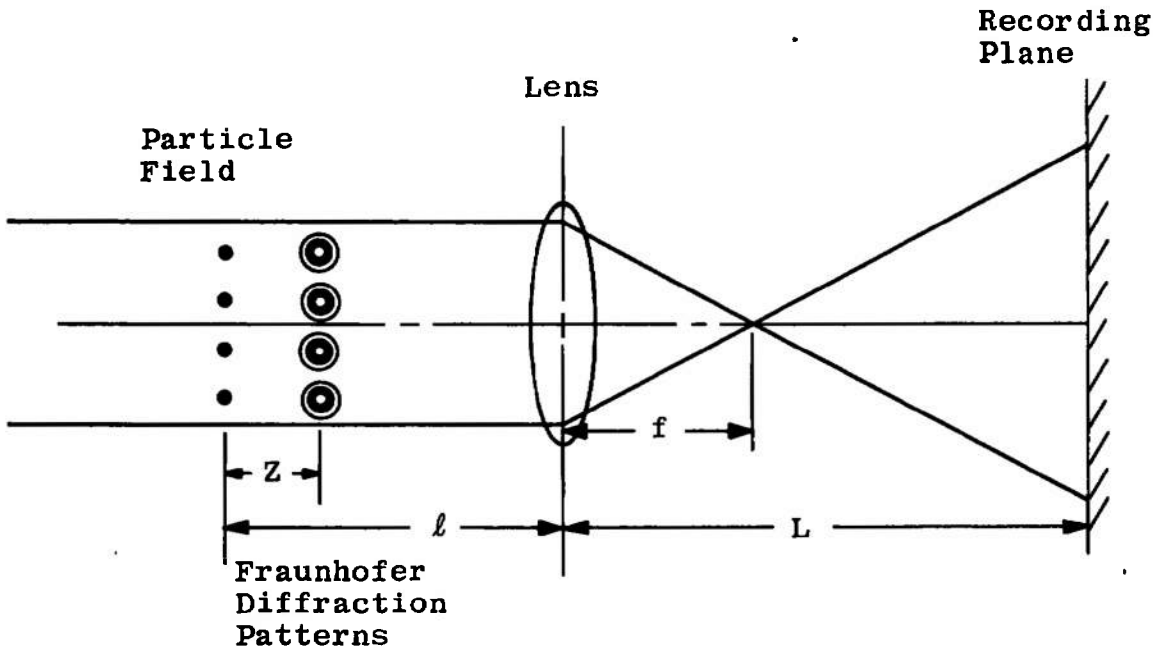

a. Diffraction Pattern Imaging

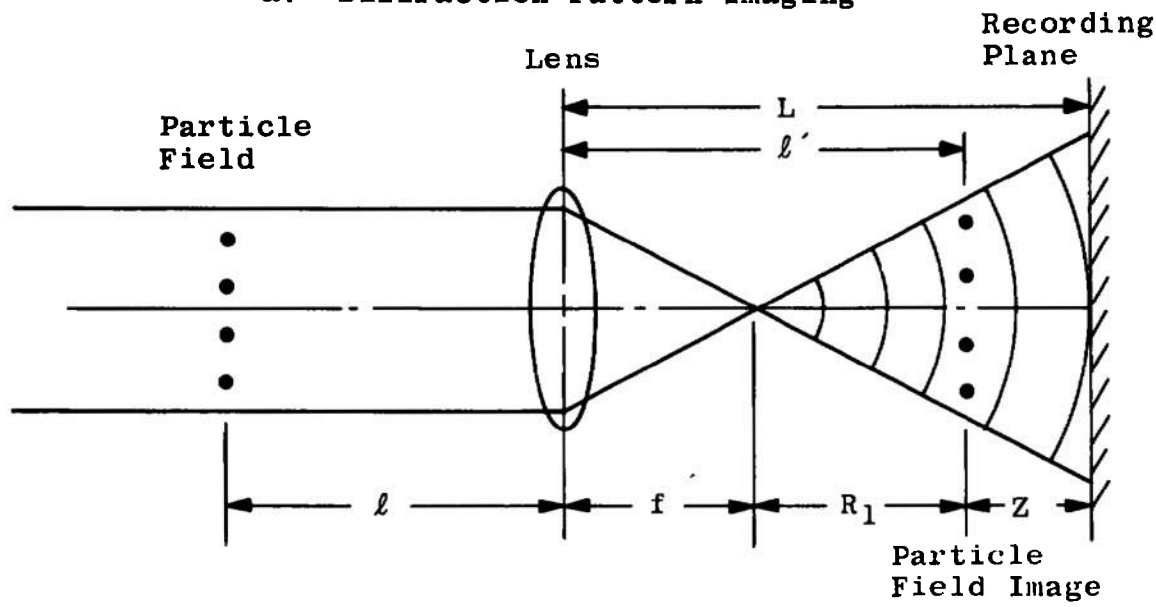

b. Particle Field Imaging

Fig. 22 Fraunhofer hologram construction using a lens to premagnify the particle field

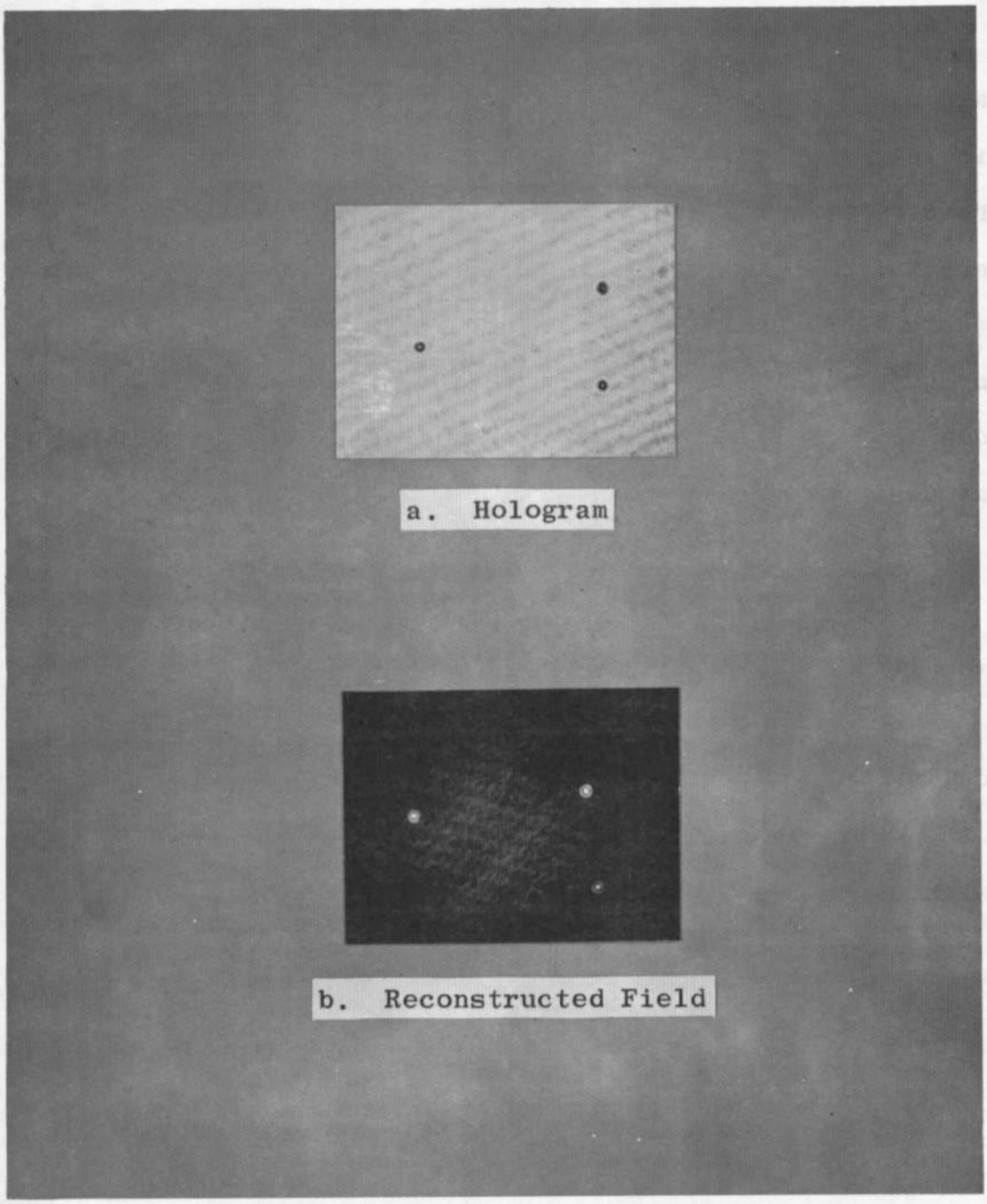

Fig. 23 Magnification of a planar particle field in the recording process with a lens where m = 6.4x

was reconstructed with plane waves and recorded approximately 85 cm from the hologram. Interference caused by the virtual image can be seen surrounding the real images of the particles. This interference is present because the patterns were recorded in the Fresnel region of the particles. The point where the real image was reconstructed in focus was difficult to determine because of its gradual intensity buildup over many centimeters. The "fuzziness" associated with out-of-focus images was not present. This behavior is much like that discussed in Section III for large particles.

4.3 MAGNIFICATION IN THE RECONSTRUCTION PROCESS

Spherical Waves

Reconstruction with spherical waves is shown schematically in Figure 20b, page 57. The magnification is related to the radius of the illuminating wave and the recording distance by

$$m_s = \frac{1}{1 - \frac{\lambda_1}{\lambda_2}\frac{Z}{R_2}} \tag{42}$$

which is from Equation 35 where $R_1 = \infty$. This equation can also be derived from Equation 37 solved for Z_2 and using the appropriate similar triangles in Figure 20b.

The reconstructed image of a particle field magnified

13.5 times with spherical waves is shown in Figure 24. The radius of the reconstructing beam was 16.2 cm and the particle field was in focus 194 cm from the hologram. Sharpness of the images is to be noted along with the reconstructed small detail. Particles diameters range from 220 μm for the larger paint particles in the center down to 15 μm for the smallest dust particles. The hologram of this particle field is shown in Section II, Figure 7, page 24.

Because of the large reconstruction distance magnification much greater than that shown in Figure 24 would be inconvenient. Also, as magnification becomes too large, the image is degraded by a lack of recorded resolution on the hologram making the magnification "empty".

According to Equation 42, large magnification can also be obtained when R_2 is less than Z. It was found that for this case, image degradation results from interference between the virtual image and real image. This can be thought of as arising from the lens-like properties of the hologram. Since Z is the focusing point of the hologram, when the point source is between it and the virtual image, the images are combined on both sides of the hologram and interfere. Thus in reconstruction, the criterion

$$R_2 \geq Z$$

must be observed to obtain clean Fraunhofer images.

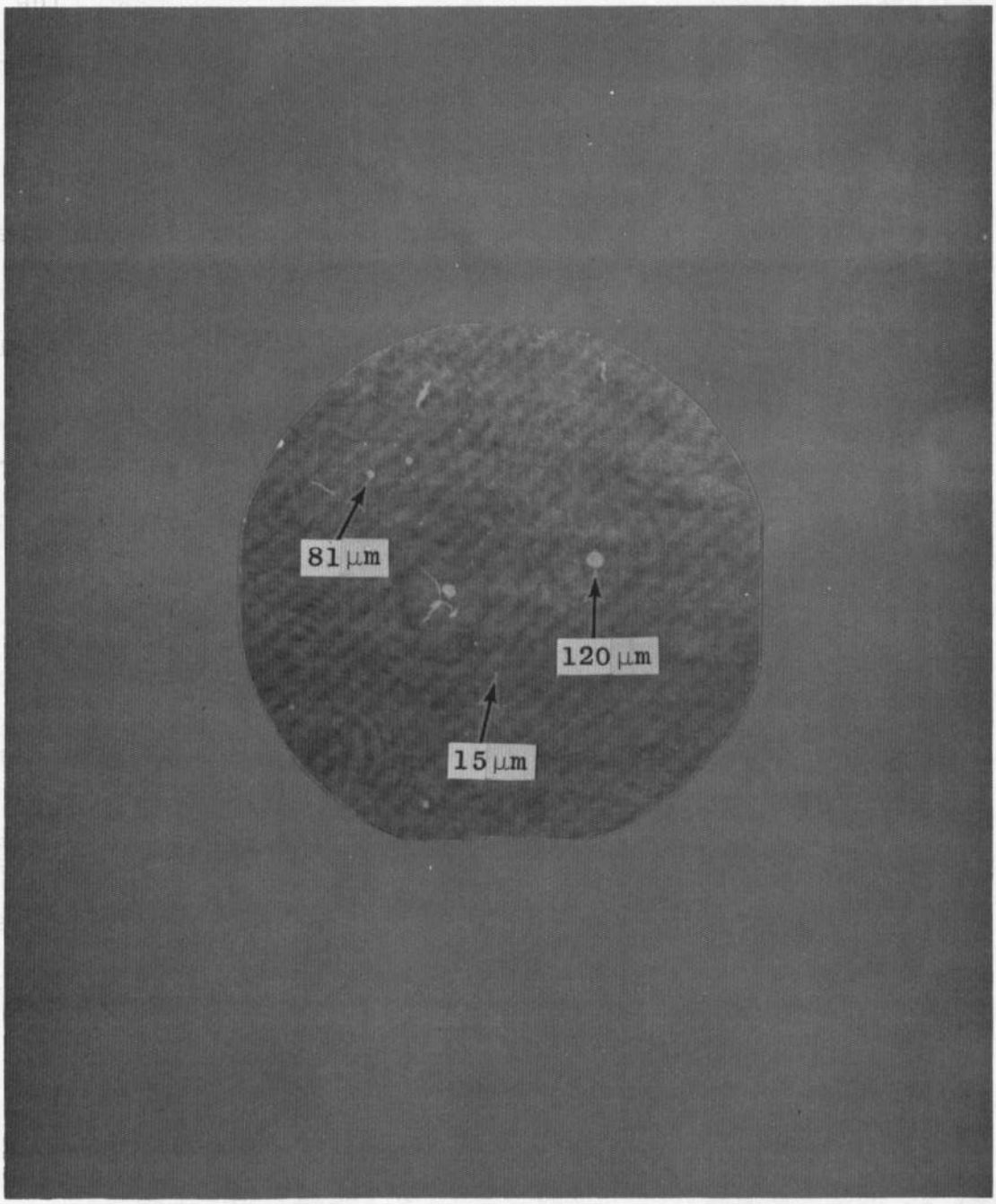

Fig. 24 Real image of a planar particle field reconstructed and magnified 13.5 times with spherical-waves

Thin Lenses

When the hologram is illuminated with plane waves, the unmagnified reconstructed images can be enlarged by an optical system. For a single thin lens, the magnification of the images is given by Equation 36. The object imaged by the lens may be either the real or virtual reconstructed images.

Figure 25 shows three stages of magnification of the real images of a field of graphite particles. The particle diameters range from 20 to 200 μm. In Figure 25a, the particle field was magnified 7.3 times by a 7.5 cm focal length lens. The central portion of this figure is shown magnified 15 times in Figure 25b. The image plane in this case was 193.5 cm from an 11.5 cm lens. This enlarged image was magnified a second time by an 8 cm lens placed near the recording plane. Other imaging systems could reduce this distance by an order of magnitude. Overall magnification was 26.2 times, and the field is shown in Figure 25c. Magnification any larger than this became "empty", resulting in blurred images and poor resolution.

An optical system, such as a microscope, could greatly reduce the observation distance of the reconstructed magnified images. All attempts, however, to directly observe the images through a 50 power microscope have been fruitless. Particles could only be seen as blurs of light. It is believed that this is due to the limiting aperture effect of

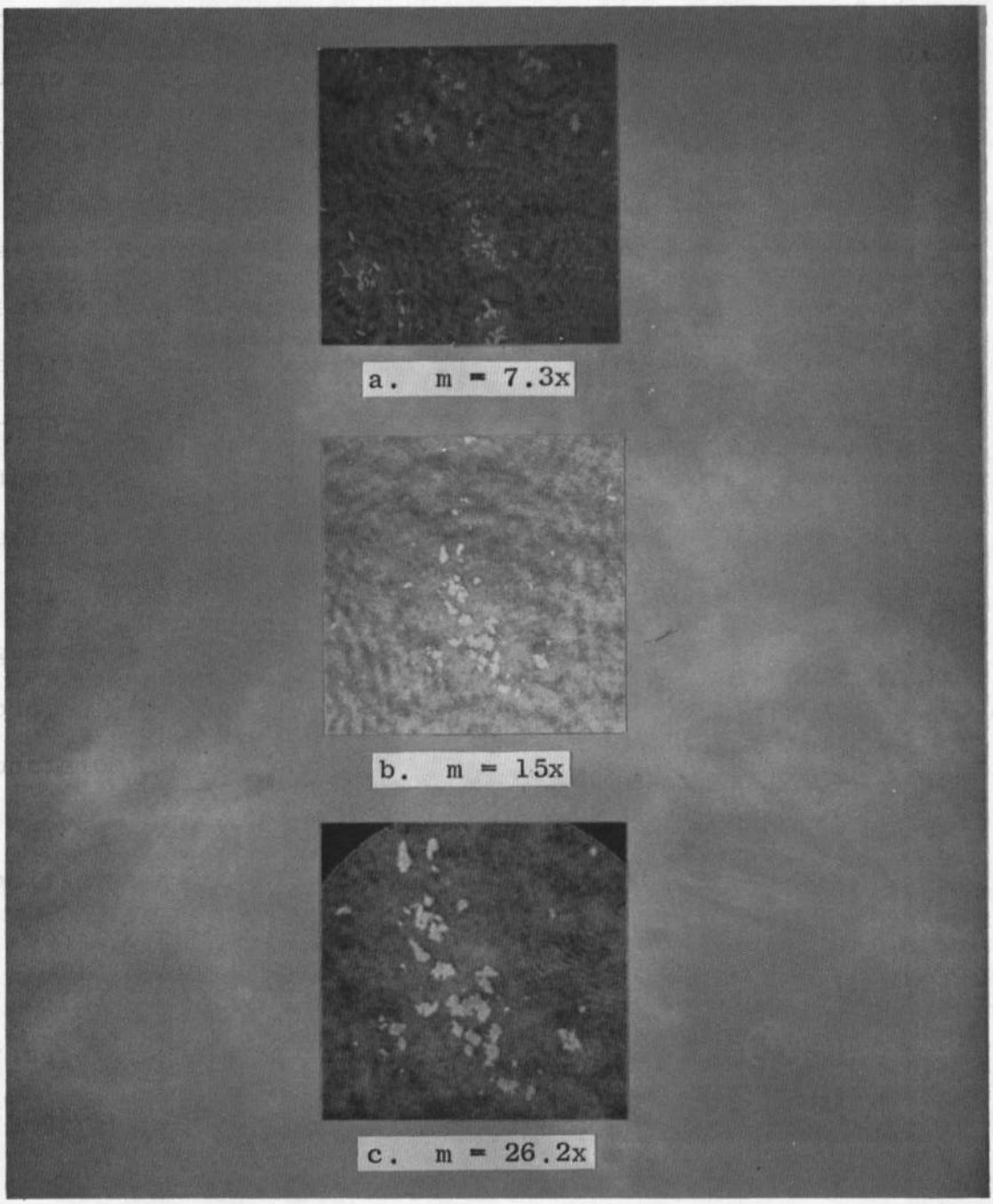

Fig. 25 Graphite particle field recorded and reconstructed with plane waves and magnified during reconstruction with a lens system

the microscope objective. The cone of rays intercepted by this lens is empty of the particle information necessary to resolve the fine detail. However, focusing the images onto a frosted glass plate placed in the object field of the microscope allowed them to be observed when the objective was focused on the plate. Fine object detail in this case was degraded by the granularity of the frosted glass.

SECTION V
SUMMARY AND CONCLUSIONS

Two techniques have been described which are capable of furnishing data for measuring the location and size of particles within a three-dimensional field. Both techniques are based on photographically recording the interference between the light diffracted by the particle and the partially coherent background, or undiffracted light. When the interference patterns are recorded in the far-field (Fraunhofer) region of the particles, the particle parameters may be calculated directly from the densitometer traces of the fringes, or the particle field may be reconstructed holographically and measurements taken of the images.

The far-field interference patterns were shown to be functions of the particle radius and recording distance. The theoretical predictions were verified experimentally. By measuring the density variations across the patterns with a densitometer, the location and size of the particle were determined. An error in calculating the particle location was found to result from the approximations that the Airy term of the intensity distribution can be neglected. This error can be reduced to a minimum by moving the recording plane into a larger far-field region from the particle and using the first minimum of the intensity function in the

calculations provided particle sizes and seeding density is commensurate.

The measurements of the particle radius rely on finding the first zero of the first order Bessel function in the fringe pattern. This occurs when the intensity deviates from its sinusoidal variations and goes to the background. The first zero occurs after the sine function has gone through approximately 3N quadrants with the contrast of the fringes decreasing as 1/N. N is the far-field number. For large N, therefore, the particle size information is severely limited by system noise, such as film grain, scattered light, dust particles and nonuniformity of the reference beam. Accuracy in measuring the particle radii increases, therefore, when the particles are only a few far-fields from the recording plane. Other zeroes of the Bessel function may also be used to calculate the particle size, but these are more difficult to identify.

Control of the film characteristics is essential for accurate densitometer traces of the fringe patterns. For a small film gamma, indicative of a short developing time, the large far-field number fringes will be too light to be recorded by the densitometer. However, a negative developed with a large gamma will suffer from nonlinearly recording of the first peaks of small far-field number fringe patterns. The film gamma thus limits the range of far-field number

patterns that may be studied from a single negative.

Films of low granularity should be used to record the fringes because of the errors introduced into the diffraction patterns by noise. The exposure range should also be held to a minimum on the gamma portion of the characteristic curve to reduce the graininess (15).

The particle density of the volume must be as small as possible to avoid overlapping of adjacent Fraunhofer patterns. These will produce extraneous fringes on the densitometer traces, which could obliterate the first minimum of the Bessel function. This is especially true for large N where the patterns are spread out over a large film area.

Odd-shaped particles cannot be accurately measured with this technique because of the assumed circularity for the Fourier transform. Measurements taken from unsymmetrical diffraction patterns can be averaged over each side of the pattern to yield an approximate particle size lying between the maximum and minimum particle dimensions.

The second technique for measuring particle sizes and their location in a volume follows directly from the first, since the fringe patterns constitute Fraunhofer holograms of each of the particles. The object and reference beams of the hologram are the diffracted and background light from the volume, respectively. Illuminating the developed film with plane waves of coherent light will reconstruct the particle

field exactly to size and in the same position relative to the hologram as it was recorded. Consequently, the position and size of the particles may be measured directly from the reconstructed image. The accuracy of these measurements depends on the accuracy of the measuring equipment and the ability to determine the point of focus of the image.

The holograms are recorded in the far-field region of the individual particles to eliminate interference from the virtual image. This image, which appears in the conventional (Fresnel) in-line hologram of Gabor (1), creates no problem since it reduces to a constant for the far-field approximation. Furthermore, Fraunhofer holograms are more convenient to record for small particles because of the far-field condition.

Unlike the diffraction pattern technique where circular symmetry about the particles' axis was assumed, the particles can be any shape and of any composition, since the hologram contains and reconstructs the information that is unique to the particles which scattered the radiation. Particles from perhaps 10 μm to one mm may be recorded on Fraunhofer holograms. Each hologram will only reconstruct particles free from conjugate image interference and system noise that were recorded in their far-fields from N = 1 to N = 100, respectively. Thus, the size range reconstructed from a single hologram is limited to about an order of magnitude.

Fringe overlapping on the hologram does not limit the particle information of the volume as in the previous technique. The particles will be reconstructed independently of any interference from other wavefronts. The limit of the particle density depends upon the depth of the volume and the particle scattering cross-sectional area. If the density is too large relative to the area the volume will attenuate the incident light to such a degree that the film will not accurately record the information of the particles in the volume. Depth of fields achieved in practice have been typically 50 to 60 far-field distances (7). Figure 19, page 51, illustrated the relation of the volume depth to the particle radii for various densities.

Out-of-focus images were found to be a source of difficulty when observing adjacent planes in the volume. The focusing depth of the particles increases with particle size making it difficult to ascertain in which plane the larger particles are in focus. This limits the resolvable depth of the reconstructed volume.

The gamma of the film is not as critical as it is when the diffraction patterns are studied. Images reconstructed from underexposed negatives will have poor contrast but are still observable. Too much exposure will wash out the higher frequencies of the fringe pattern and reduce the image resolution.

Magnification is introduced into one or both of the steps of recording and reconstructing the hologram to enlarge the images to an observable and measurable size. Spherical waves or lenses will magnify the particle field in either step.

Spherical waves increase the reconstruction distance and the lateral field dimensions by a factor m, as indicated by Equations 37 and 38, respectively. Recording is limited practically to planar fields since the volume depth suffers upon reconstruction from nonuniform longitudinal magnification. Also, the focusing plane of the reconstructed images is difficult to locate accurately because of the longer depth of field of the enlarged particles, and approximations to this plane must be made.

If the increase in reconstruction distance can be afforded, magnification can be applied in the recording process to a planar field to increase the detail which the film will record. This results in a better reconstructed image resolution and allows poorer resolution film to be used if necessary.

The reconstruction distance is also increased by Equation 37 when a lens is used to magnify the particle field in the recording process. The magnified image can be thought of as being illuminated with spherical waves arising from the focal point of the lens (Figure 22, page 63). Therefore,

the disadvantages and advantages of spherical wave recording will apply here. The lens aperture could also be a factor in limiting the resolution of the smaller particles (11).

Spherical wave reconstruction of a Fraunhofer hologram recorded with plane waves yields magnifications which are much greater than are possible with spherical wave recording and plane wave reconstruction. When the reconstructing point source approaches the recording distance, the magnification will increase according to Equation 42. Thus, planes within the volume are magnified differently upon reconstruction and will not be reconstructed in the same relation as they were recorded.

A lens placed behind the hologram when it is illuminated with plane waves overcomes the disadvantages of the previous magnification techniques and allows the location of the particles, as well as their size, to be determined more accurately. Since the hologram is illuminated with plane waves, the volume is reconstructed exactly as it was recorded. By moving the hologram, individual planes of the reconstructed volume will be magnified and imaged by the lens. Since the positions of the lens system and observation plane are not changed, the magnification of the particles in each plane focused will remain constant. The location of the planes relative to one another is simply determined by measuring the distance the hologram is moved in order to bring each plane

into focus. The distance of the hologram from the object plane of the lens is Z, the recording distance of the volume.

Magnification is increased by increasing the observation plane distance from the lens. This distance can be reduced for larger magnification by using a short focal length lens. Unfortunately, a lens of this sort usually has a small numerical aperture associated with it, which results in poor image resolution.

Any appreciable magnification in the reconstruction is limited by the resolution of the recording process. When this limit is exceeded the images reconstruct empty of any resolution with a corresponding loss of contrast. Film resolution and lack of coherence of the illuminating light source cause the image to be degraded. When the path difference between the background and the diffracted light is longer than the coherence length of the source, the phase information in the diffracted light will no longer be recorded. This reduces the effective size of the hologram of each particle, thereby decreasing the image resolution. Coherence requirements of the laser were not considered in this investigation since the coherence lengths of commercially available lasers are sufficient to record objects with the 100 far-field distance limit set on the hologram for clean reconstructions (16). Therefore, the resolution of the hologram system depends on the resolution of the film used to record the hologram in the plane wave case.

BIBLIOGRAPHY

1. Gabor, D. "Microscopy by Reconstructed Wavefronts," Proceedings of the Royal Society, A197:454-487, March, 1949.

2. Thompson, B. J. "Diffraction by Opaque and Transparent Particles," Society of Photo-Optical Instrumentation Engineers Journal, 2:43-46, December, 1963-January, 1964.

3. Parrent, G. B., and B. J. Thompson. "On the Fraunhofer (Far-Field) Diffraction Patterns of Opaque and Trans-Parent Objects with Coherent Background," Optica Acta, 11:183-194, July, 1964.

4. Ward, J. "Laser Fog Disdrometer System," Air Force Cambridge Research Laboratories Report No. AD656-487, Bedford, Massachusetts, June, 1967.

5. DeVelis, J. B., G. B. Parrent, and B. J. Thompson. "Image Reconstruction with Fraunhofer Holograms," Journal of the Optical Society of America, 56:423-427, April, 1966.

6. Thompson, B. J. "A New Method of Measuring Particle Size by Diffraction Techniques," Japanese Journal of Applied Physics, 4:302-307, Supplement 1, 1965.

7. Thompson, B. J., J. H. Ward, and W. R. Zinky. "Application of Hologram Techniques for Particle Size Analysis," Applied Optics, 6:519-526, March, 1967.

8. Thompson, B. J., and J. H. Ward. "Particle Sizing--The First Direct Use of Holography," Scientific Research, 1:37-40, October, 1966.

9. Thompson, B. J., G. B. Parrent, J. H. Ward, and B. Justh. "A Readout Technique for the Laser Fog Disdrometer," Journal of Applied Meteorology, 5:343-348, June, 1966.

10. DeVelis, J. B., and G. O. Reynolds. Theory and Applications of Holography. Reading, Massachusetts: Addison-Wesley Publishing Company, 1967.

11. Born, M., and E. Wolf. Principles of Optics. New York: Pergamon Press, 1965.

12. Silver, S. Microwave Antenna Theory and Design. Massachusetts Institute of Technology Radiation Laboratory Series, No. 12. Boston, Massachusetts: Boston Technical Publishers, 1967.

13. Stroke, G. W. An Introduction to Coherent Optics and Holography. New York: Academic Press, 1966.

14. Glasstone, S. Textbook of Physical Chemistry. Princeton, New Jersey: D. Van Nostrand Company, 1959.

15. Kodak Plates and Film for Science and Industry. Kodak Publication No. P-9, Rochester, New York: Eastman Kodak Company, 1967.

16. Reynolds, G. O., and J. B. DeVelis. "Hologram Coherence Effects," Institute of Electrical and Electronic Engineers Transactions on Antennas and Propogation, AP-15:41-48, January, 1967.

UNCLASSIFIED

Security Classification

DOCUMENT CONTROL DATA - R & D

(Security classification of title, body of abstract and indexing annotation must be entered when the overall report is classified)

1. ORIGINATING ACTIVITY (Corporate author)	2a. REPORT SECURITY CLASSIFICATION
Arnold Engineering Development Center ARO, Inc., Operating Contractor Arnold Air Force Station, Tenn. 37389	UNCLASSIFIED
	2b. GROUP N/A

3. REPORT TITLE

ANALYSIS OF THE TECHNIQUES FOR MEASURING PARTICLE SIZE AND DISTRIBUTION FROM FRAUNHOFER DIFFRACTION PATTERNS

4. DESCRIPTIVE NOTES (Type of report and inclusive dates)

Final Report September 1967 to March 1968

5. AUTHOR(S) (First name, middle initial, last name)

Ronald A. Belz, ARO, Inc.

6. REPORT DATE	7a. TOTAL NO. OF PAGES	7b. NO. OF REFS
September 1968	92	16

8a. CONTRACT OR GRANT NO.	9a. ORIGINATOR'S REPORT NUMBER(S)
F40600-69-C-001 b. PROJECT NO. 8219 c. Task 821907 d. Program Element 6240533F	AEDC-TR-68-125 9b. OTHER REPORT NO(S) (Any other numbers that may be assigned this report) N/A

10. DISTRIBUTION STATEMENT

This document has been approved for public release and sale; its distribution is unlimited.

11. SUPPLEMENTARY NOTES	12. SPONSORING MILITARY ACTIVITY
Available in DDC.	Arnold Engineering Development Center (AETS), Arnold Air Force Station, Tennessee 37389

13. ABSTRACT

The location and size of particles within a volume which is stationary or dynamic can be found by two techniques of coherent optics. In the first technique the volume is illuminated with coherent light and the resulting diffraction patterns are recorded in the far-field (Fraunhofer region) of the particles. The particle information is found from the resultant density variations on the film. In the second technique the developed negative (a Fraunhofer hologram) is illuminated with coherent light and the particle field is reconstructed in three dimensions. This investigation is an analysis of these two techniques and their relative merits. Because magnification is important in the second technique the methods of magnifying the volume are discussed. It is found that reconstructing the volume from the hologram yields particle information which is easier to obtain than the information resulting from the diffraction patterns. The volume is also found to be easily and uniformly magnified by an imaging lens in the reconstruction process.

DD FORM 1 NOV 65 1473

UNCLASSIFIED

Security Classification

14. KEY WORDS	LINK A		LINK B		LINK C	
	ROLE	WT	ROLE	WT	ROLE	WT
1 lasers 2 holograms Fraunhofer patterns 3 particle size optics, coherent 4: Particles -- Size 15-18						